

**A Feasibility Study of Diffusion Weighted Imaging
and Parametric Response Map Analysis for Treatment Response
Prediction in Nasopharyngeal Cancer**

Miss Titiya Jirawatwanith



**A Thesis Submitted in Partial Fulfillment of the Requirements
for the Degree of Master of Science in Medical Physics
Department of Radiology
FACULTY OF MEDICINE
Chulalongkorn University
Academic Year 2019
Copyright of Chulalongkorn University**

การศึกษาความเป็นไปได้ของการตรวจด้วยคลื่นแม่เหล็กไฟฟ้าโดยอาศัยเทคนิค
การเคลื่อนที่ของโมเลกุลน้ำในเนื้อเยื่อและการวิเคราะห์แบบพารามตริกเรสปอนส์แมพ
เพื่อทำนายผลการรักษาในโรคมะเร็งคอหอยหลังโพรงจมูก



วิทยานิพนธ์นี้เป็นส่วนหนึ่งของการศึกษาตามหลักสูตรปริญญาวิทยาศาสตรมหาบัณฑิต
สาขาวิชาฟิสิกส์การแพทย์ ภาควิชารังสีวิทยา
คณะแพทยศาสตร์ จุฬาลงกรณ์มหาวิทยาลัย
ปีการศึกษา 2562
ลิขสิทธิ์ของจุฬาลงกรณ์มหาวิทยาลัย

Thesis Title A Feasibility Study of Diffusion Weighted Imaging and
 Parametric Response Map Analysis for Treatment
 Response Prediction in Nasopharyngeal Cancer
By Miss Titiya Jirawatwanith
Field of Study Medical Physics
Thesis Advisor Assistant Professor YOTHIN RAKVONGTHAI, Ph.D.

Accepted by the FACULTY OF MEDICINE, Chulalongkorn University in
Partial Fulfillment of the Requirement for the Master of Science

..... Dean of the FACULTY OF
 MEDICINE
(Professor SUTTIPONG WACHARASINDHU, M.D.)

THESIS COMMITTEE

..... Chairman
(Associate Professor ANCHALI KRISANACHINDA,
Ph.D.)
..... Thesis Advisor
(Assistant Professor YOTHIN RAKVONGTHAI, Ph.D.)
..... External Examiner
(Associate Professor Kosuke Matsubara, Ph.D.)



จุฬาลงกรณ์มหาวิทยาลัย
CHULALONGKORN UNIVERSITY

จิตติยา จิรวัดน์วนิชย์ : การศึกษาความเป็นไปได้ของการตรวจด้วยคลื่นแม่เหล็กไฟฟ้าโดยอาศัยเทคนิค การเคลื่อนที่ของโมเลกุลน้ำในเนื้อเยื่อและการวิเคราะห์แบบพารามตริกเรสพอนส์แมพ เพื่อทำนายผลการรักษาในโรคมะเร็งคอหอยหลังโพรงจมูก. (A Feasibility Study of Diffusion Weighted Imaging and Parametric Response Map Analysis for Treatment Response Prediction in Nasopharyngeal Cancer) อ.ที่ปรึกษาหลัก : ศศ. ดร.โยธิน รักงษ์ไทย

เทคนิคการสร้างภาพที่แสดงการเคลื่อนที่ของโมเลกุลน้ำ (Diffusion-weighted imaging หรือ DWI) เป็นเทคนิคหนึ่งที่ใช้กันอย่างแพร่หลายในเครื่องตรวจคลื่นแม่เหล็กไฟฟ้า (Magnetic Resonance Imaging หรือ MRI) ที่แสดงคุณสมบัติการเคลื่อนที่ของโมเลกุลน้ำในเนื้อเยื่อ การเปลี่ยนแปลงของสัมประสิทธิ์การแพร่ปรากฏ (Apparent Diffusion Coefficient หรือ ADC) ที่ได้มาจากภาพ DWI ได้ถูกนำมาใช้เป็นตัวบ่งชี้ทางชีวภาพเพื่อทำนายผลการตอบสนองต่อการรักษาในคนไข้โรคมะเร็งได้ อย่างไรก็ตาม วิธีนี้อาศัยค่าเฉลี่ยการเปลี่ยนแปลงของค่าโมเลกุลน้ำในก้อนมะเร็งซึ่งไม่สอดคล้องกับความไม่เป็นเนื้อเดียวกัน (heterogeneity) ในก้อนมะเร็ง ที่แต่ละส่วนจะมีความหลากหลายทางชีวภาพต่างกัน เพื่อที่จะแก้ปัญหานี้ ได้มีการเสนอตัวบ่งชี้ทางชีวภาพด้วยวิธีใหม่ขึ้น เรียกว่าพารามตริกเรสพอนส์แมพ (Parametric Response Map หรือ PRM) โดย PRM นี้จะบอกการเปลี่ยนแปลงของโมเลกุลน้ำในเนื้อเยื่อในแต่ละว็อกเซล (voxel) ในงานวิจัยนี้ เราศึกษาการใช้วิธีการวิเคราะห์ด้วย PRM บนค่าของ ADC ที่ได้จาก DWI เพื่อทำนายผลของการรักษาในคนไข้โรคมะเร็งคอหอยหลังโพรงจมูก ในขั้นตอนการวิจัย ผู้วิจัยเก็บข้อมูลภาพจากผู้ป่วยโรคมะเร็งคอหอยหลังโพรงจมูกที่รักษาและติดตามผลการรักษาที่โรงพยาบาลจุฬาลงกรณ์ ทั้งหมด 26 ราย โดยเป็นผู้ป่วยที่มีการตอบสนองต่อการรักษาดี (complete response หรือ CR) 20 ราย และผู้ป่วยที่มีการตอบสนองต่อการรักษาบางส่วน (partial response หรือ PR) 6 ราย ข้อมูลภาพของผู้ป่วยแต่ละคนประกอบไปด้วยภาพ DWI และ ADC ที่ก่อนการรักษาและที่สัปดาห์ที่ห้าหลังจากการให้ยาเคมีบำบัดร่วมกับการฉายรังสี ภาพของทั้งสองช่วงเวลาจะถูกนำมาลงทะเบียนภาพ (registration) และเปรียบเทียบกัน ซึ่งเราสามารถคำนวณตัวบ่งชี้ทางชีวภาพ PRM₊ ที่มีนิยามว่า สัดส่วนของว็อกเซลที่มีค่า ADC เพิ่มขึ้นเทียบกับจำนวนว็อกเซลของก้อนมะเร็งที่เป็นเปอร์เซ็นต์ เพื่อยืนยันความเป็นไปได้ในการใช้ PRM₊ เราได้คำนวณค่าเฉลี่ยและส่วนเบี่ยงเบนมาตรฐานของ PRM₊, เปอร์เซ็นต์การเปลี่ยนแปลงของปริมาตร (% Δ Vol) และ เปอร์เซ็นต์การเปลี่ยนแปลงของสัมประสิทธิ์การแพร่ปรากฏ (% Δ ADC) ในคนไข้กลุ่ม CR และกลุ่ม PR โดยเป็นการแบ่งกลุ่มจากการประเมินการตอบสนองต่อการรักษาหลังจบการรักษาเป็นเวลาหกเดือนตามหลักเกณฑ์ของ RECIST 1.1 เราประเมินความแตกต่างกันทางสถิติของค่าตัวบ่งชี้ทางชีวภาพทั้งสามในผู้ป่วยสองกลุ่มด้วยการทดสอบแบบ t-test และสร้างเส้นโค้งอาร์โอซี (receiver operating characteristic curve หรือ ROC curve) เพื่อวัดความสามารถในการทำนายผลการตอบสนองต่อการรักษาของตัวบ่งชี้ทางชีวภาพเทียบกับกับการเดาสุ่มด้วยการทดสอบแบบ Mann-Whitney's U-test ผลการศึกษาพบว่าใน % Δ Vol และ % Δ ADC ของคนไข้ทั้งสองกลุ่มไม่มีนัยยะสำคัญกันทางสถิติ ในทางตรงกันข้าม PRM₊ ของคนไข้ทั้งสองกลุ่มนั้นมีนัยสำคัญทางสถิติ ($80.5 \pm 8.5\%$ ใน CR เทียบกับ $70.2 \pm 7.1\%$ ใน PR, $p < 0.05$) ในส่วนของการเปรียบเทียบความสามารถในการทำนายผลการตอบสนองต่อการรักษาพบว่า PRM₊ มีค่าพื้นที่ใต้เส้นโค้งอาร์โอซี (AUC) มีค่ามากกว่าเมื่อเทียบกับตัวบ่งชี้ทางชีวภาพตัวอื่น (0.817, 0.633 และ 0.417 ในตัวบ่งชี้ทางชีวภาพ PRM₊, % Δ ADC และ % Δ Vol ตามลำดับ) และ พบว่ามีเพียงค่า PRM₊ ที่ทำนายผลแตกต่างจากการเดาสุ่มอย่างมีนัยสำคัญทางสถิติ ($p < 0.05$) ผลการศึกษาสรุปได้ว่า PRM₊ ที่เสนอจาก ADC อาจเป็นตัวบ่งชี้ทางชีวภาพที่มีศักยภาพสำหรับการทำนายการตอบสนองต่อการรักษาในผู้ป่วยโรคมะเร็งคอหอยหลังโพรงจมูก

สาขาวิชา ฟิสิกส์การแพทย์
ปีการศึกษา 2562

ลายมือชื่อนิติศ
ลายมือชื่อ อ.ที่ปรึกษาหลัก

6174007430 : MAJOR MEDICAL PHYSICS

KEYWORD: Magnetic Resonance Imaging (MRI), Diffusion Weighted Imaging (DWI), Parametric Response Map (PRM), Nasopharyngeal Cancer

Titiya Jirawatwanith : A Feasibility Study of Diffusion Weighted Imaging and Parametric Response Map Analysis for Treatment Response Prediction in Nasopharyngeal Cancer . Advisor: Asst. Prof. YOTHIN RAKVONGTHAI, Ph.D.

Diffusion-weighted imaging (DWI) is an MRI technique which provides functional information of tissue by detecting microscopic motion of water molecules. The change of apparent diffusion coefficient (ADC) derived from DWI was used as an imaging biomarker for treatment response prediction in cancers. However, it was based on whole-tumor analysis which did not reflect heterogeneity within the tumor. To overcome this limitation, a new method called parametric response map (PRM) analysis was proposed to evaluate response by quantifying voxel-wise changes in ADC. Here we investigated the use of PRM analysis on ADC from DWI as an imaging biomarker for treatment response prediction in nasopharyngeal carcinoma (NPC) patients. We collected twenty-six patient datasets including twenty complete response (CR) patients and six partial response (PR) patients at King Chulalongkorn Memorial Hospital where one patient dataset consisted of DWI and ADC data acquired before (i.e. pre-treatment) and at five weeks after initiation of chemoradiation therapy (i.e. mid-treatment). For each dataset, we compared pre-treatment ADC image with co-registered mid-treatment ADC image, and calculated PRM_+ which was defined as the percentage of voxels with increased ADC values with respect to total voxels within the tumor ROI. To validate the feasibility of the PRM biomarker, we computed the mean and standard deviation (SD) of percentage change in tumor volume ($\% \Delta Vol$) and in ADC ($\% \Delta ADC$) and PRM_+ across CR and PR patients classified by RECIST1.1 guideline at 6 months. We determined if each of the three biomarker yielded difference between the two patients groups using t-test. To evaluate outcome prediction performance for each biomarker, we constructed the receiver operating characteristic (ROC) and compared with random guessing using Mann-Whitney's U-test. The results showed that no significant difference in $\% \Delta Vol$ and in $\% \Delta ADC$ between CR and PR groups. In contrast, PRM_+ was significantly different between CR and PR groups ($80.5 \pm 8.5\%$ in CR vs $70.2 \pm 7.1\%$ in PR, $p < 0.05$). In terms of prediction performance, PRM_+ has higher AUC value than both $\% \Delta ADC$ and $\% \Delta Vol$ (0.817, 0.633, and 0.417 for PRM_+ , $\% \Delta ADC$ and $\% \Delta Vol$, respectively). Only PRM_+ was significantly different from random guessing ($p < 0.05$). Our results implied that the proposed PRM_+ from ADC could be a potential biomarker for early treatment response prediction in NPC patients.

Field of Study: Medical Physics
Academic Year: 2019

Student's Signature
Advisor's Signature

ACKNOWLEDGEMENTS

The success of this thesis depends on the contribution of many people. First, I would like to express my sincere gratitude to my advisor Assistant Professor Yothin Rakvongthai, Division of Nuclear Medicine, Department of Radiology, Faculty of Medicine, Chulalongkorn University for support my master degree study and research with patience, helpful, supervision and motivation during the whole study. Without his opportunity and assistance involvement in every step throughout the process, this thesis would have never been accomplished.

Besides my advisor, I owe my deepest gratitude to Nutchawan Jittapiromsak, M.D. and Thidaporn Tangyoosuk, M.D., Division of Diagnostic Radiology, King Chulalongkorn Memorial Hospital who devote precious time for greatly assisting the collection of my data and suggesting for the clinical research part.

I profoundly and profusely thank my thesis committee: Associate Professor Anchali Krisanachinda, Division of Nuclear Medicine, Department of Radiology, Faculty of Medicine, Chulalongkorn University Chairman of my thesis committee, and Associate Professor Kosuke Matsubara, Ph.D., Kanazawa University, Japan external examiner of thesis defense for their encouragement and insightful comments which incited me to widen my research from various perspectives.

My sincere thanks also go to Associate Professor Sivalee Suriyapee, Chief of Physicist and Sornjarod Oonsiri, Ph.D., and Mananchaya Vimolnoch, MSc. at Division of Radiation Oncology, King Chulalongkorn Memorial Hospital for helpful suggestions, offering me phantom, and contribution for quality control part. I would also like to thank the technicians of MRI simulator for their kindness and assistance in this work.

I am deeply grateful to all the lecturers, staff and my colleagues in the Master of Science program in Medical Physic, Department of Radiology, Faculty of Medicine, Chulalongkorn University for their suggestion, kindly support and teaching through the whole study.

In addition, a thank you to my research group members in Chulalongkorn University Biomedical Imaging Group (CUBIG) for their energy, understanding, and help throughout my work for all two years.

Finally, I would like to thank my family for their support and encouragement during the compilation of this dissertation. They kept me going on and this work would not have been possible without their input.

Titiya Jirawatwanith

TABLE OF CONTENTS

	Page
ABSTRACT (THAI)	iii
ABSTRACT (ENGLISH).....	iv
ACKNOWLEDGEMENTS	v
TABLE OF CONTENTS.....	vi
LIST OF TABLES	ix
LIST OF FIGURES	x
LIST OF ABBREVIATION.....	xii
CHAPTER I INTRODUCTION.....	1
1.1 Background and rationale	1
1.2 Research questions.....	2
1.2.1 Primary question.....	2
1.2.2 Secondary question.....	2
1.3 Research objective	2
1.3.1 Primary objective	2
1.3.2 Secondary objective	2
1.4 Significance and impact of the work	2
1.5 Definition.....	2
CHAPTER II THEORY AND RELATED LITERATURE	4
2.1 Theory.....	4
2.1.1 Magnetic resonance imaging (MRI).....	4
2.1.1.1 Diffusion-weighted imaging (DWI).....	4
2.1.2 Biomarker	7
2.1.3 Parametric Response Map (PRM).....	8
2.1.4 Image processing.....	8
2.1.4.1 Image segmentation.....	9

2.1.4.2 Image registration.....	10
2.1.5 Nasopharyngeal carcinoma (NPC).....	11
2.1.5.1 Causes of nasopharyngeal carcinoma.....	11
2.1.5.2 Signs and symptoms of nasopharyngeal carcinoma.....	11
2.1.5.3 Radiological staging.....	12
2.1.5.4 Treatment.....	12
2.2 Review of related literatures.....	14
CHAPTER III RESEARCH METHODOLOGY	18
3.1 Research design	18
3.2 Research design model	18
3.3 Conceptual framework.....	18
3.4 Key Word.....	19
3.5 The sample.....	19
3.5.1 Target population	19
3.5.2 Sample population.....	19
3.5.3 Eligible criteria	19
3.5.3.1 The inclusion criteria.....	19
3.5.3.2 The exclusion criteria	19
3.5.4 Sample size determination.....	20
The sample size was determined according to the formula.....	20
3.6 Materials	21
3.6.1 Magnetic resonance imaging simulator	21
3.6.2 3D Slicer software	21
3.6.3 Image J software.....	22
3.6.4 MATLAB software	22
3.7 Methods	22
3.7.1 Patient data collection	22
3.7.2 Data analysis.....	23
3.7.2.1 Region of interest analysis.....	23

3.7.2.2 ADC analysis.....	24
3.7.2.3 PRM analysis.....	24
3.7.3 Classification	27
3.8 Statistical analysis.....	27
3.9 Ethical consideration	27
Chapter IV RESULTS	29
4.1 Quality control of MRI system.....	29
4.2 Patient data.....	29
4.3 Response Prediction.....	33
4.4 ROC analysis	37
Chapter V DISCUSSION AND CONCLUSIONS.....	40
5.1 Discussion.....	40
5.2 Conclusion	43
APPENDIX A Quality control of MRI system.....	44
APPENDIX B The approval of institutional review board	57
APPENDIX C Case record form	59
REFERENCES	63
VITA.....	67

LIST OF TABLES

	Page
Table 1 TNM staging of cancer by AJCC	13
Table 2 Overview of 4 literatures	17
Table 3 Clinical characteristic of patients.....	29
Table 4 Treatment response of % Δ Volume, % Δ ADC and PRM ₊	34
Table 5 Data collection of each NPC patients	35
Table 6 ROC curve correlated with treatment outcome	38
Table 7 Youden's J index and optimal cut of point of % Δ Volume, % Δ ADC and PRM ₊	39
Table 8 The comparison of biomarker results between the literature review and this study.....	42
Table 9 The percent integral uniformity (PIU) of the T1 and T2 FS image.....	46
Table 10 The results of high contrast resolution in line pair/cm.	48
Table 11 The target diameters and hole depths of the phantom	49
Table 12 Mean value of pixel intensity for low contrast sensitivity in T1 and T2FS sequence.....	50
Table 13 The result of slice geometry.....	52
Table 14 The results of geometric distortion in X and Y direction.	54
Table 15 The results of geometric distortion in Z direction.	54
Table 16 The result of percentage distortion	55
Table 17 Overview of parameters for QC testing	56
Table 18 A format of case record form for collect the patient data.	59
Table 19 A format of data collection	61
Table 20 A format of test result variable	62

LIST OF FIGURES

	Page
Figure 1 Simplified MRI spin echo pulse sequences of DWI ⁽⁴⁾	4
Figure 2 The relationship of relative signal intensity of the regions of interest in the diffusion-weighted image (Y-axis) and diffusion sensitivity or b-value (X-axis) ⁽⁷⁾	5
Figure 3 The DWI (a) and ADC (b) image of MRI brain. The red circle is highlighting abnormality (a stroke region) in the brain ⁽⁹⁾	7
Figure 4 Image processing system ⁽¹⁷⁾	8
Figure 5 (a) Original image of retinal vessel, (b) image after registration in thresholding technique ⁽²⁰⁾	9
Figure 6 Intermodal registration CT (cyan color) and transformed MRI (red color). (a) unregistered image, (b) registered image ⁽²¹⁾	10
Figure 7 Representative patients with HNSCC stratified by PRM as a responder (top row) and a non-responder (bottom row) at the time of analysis. The scatter plots show the distribution of changes in PRM throughout the entire volume of interest. Voxels with significantly increasing, decreasing, or unchanged are coded as red, blue, and green dots, respectively ⁽³²⁾	15
Figure 8 Receiver operating characteristic curve of treatment response in percentage change in tumor volume (red), mean ADC values (blue) and PRM analysis which exhibited a significant increase in ADC (green).....	16
Figure 9 Research design	18
Figure 10 Conceptual framework	18
Figure 11 MRI Simulator GE Medical systems at KCMH.....	21
Figure 12 3D Slicer software	21
Figure 13 Image J software.....	22
Figure 14 A series of MRI image in patient data set at pre-and mid-treatment.....	23
Figure 15 Image of ROI on DWI image in 3D slicer program.....	24
Figure 16 ADC image of mid-treatment in (a) the original image and (b) the registered image.	25

Figure 17 Construction of PRM of ADC are built by using tumor images at pre- and mid-treatment, a difference image is calculated. A significant decrease, increase, and no change in ADC is labelled in blue, red, and green.....	26
Figure 18 A representative case of CR patients. (a) Axial view of ADC phase at pre-treatment of nasopharynx. (b) mid-treatment ADC image at 5 weeks after CCRT started. (c) PRM overlaid on unregistered ADC image at pre-treatment. (d) The scatter plot illustrates the distribution of changes in PRM throughout the entire volumes of interest. Voxels with significant increase, unchange, or decrease in ADC values are assigned as red (92.4%), green (4.1%) and blue (3.6%), respectively.	31
Figure 19 A representative case of PR patients. (a) Axial view of ADC phase at pre-treatment of nasopharynx. (b) mid-treatment ADC image at 5 weeks after CCRT started. (c) PRM overlaid on unregistered ADC image at pre-treatment. (d) The scatter plot illustrates the distribution of changes in PRM throughout the entire volumes of interest. Voxels with significant increase, unchange or decrease in ADC values are assigned as red (63.0%), green (7.3%) and blue (29.7%), respectively.	32
Figure 20 The box plot of three biomarkers: the percentage change of volume (% Δ Vol), the percentage change of ADC (% Δ ADC) and the percentage of voxel with significant increase ADC (PRM ₊). The significant difference between both groups of patients was as assessed by t-test with $p < 0.05$	33
Figure 21 Receiver operating characteristic (ROC) curves of PRM ₊ (orange line), % Δ ADC (pink line) and % Δ Vol (purple line) for predicting treatment response in twenty-six patients with NPC. Area under ROC curves were 0.817, 0.633, and 0.417, respectively.	37
Figure 22 Magphan® SMR 170 phantom.....	44
Figure 23 The localizer image of the phantom Magphan with slice locations for axial scans indicated.	45
Figure 24 The Magphan® housing without the test cube.....	46
Figure 25 High resolution pattern.....	48
Figure 26 Low contrast pattern.....	49
Figure 27 Scan Slice geometry pattern with location of X and Y ramp.....	51
Figure 28 Geometric distortion (spatial linearity) pattern distance X and Y.	53
Figure 29 Geometric distortion (spatial linearity) pattern distance left and right.	53

LIST OF ABBREVIATION

ADC	Apparent diffusion coefficient
AJCC	American Joint Committee on Cancer
AUC	Area under the curve
B ₀	Main magnetic field
CCRT	Concurrent chemoradiation therapy
CT	Computed tomography
DCE	Dynamic contrast enhanced
DWI	Diffusion-weighted imaging
EBV	Epstein-Barr virus
EPI	Echo-planar imaging
fMRI	Functional magnetic resonance imaging
HNSCC	Head and neck squamous cell carcinoma
MRI	Magnetic resonance imaging
NPC	Nasopharyngeal carcinoma
PET	Positron emission tomography
PRM	Parametric response map
PWI	Perfusion-weighted imaging
RECIST	Response evaluation criteria in solid tumors
RF	Radiofrequency
ROC	Receiver operating characteristic curve
ROI	Region of interest
SNR	Signal to noise ratio
T	Tesla
T ₁	Longitudinal relaxation
T ₂	Transverse relaxation
TE	Echo time
TR	Repetition time
UDM	Uni-dimensional measurements

CHAPTER I

INTRODUCTION

1.1 Background and rationale

Nasopharyngeal carcinoma (NPC) is a rather common malignant tumor among Asians, especially in male patients living in Southeast Asia ⁽¹⁾. Due to anatomic locations of the nasopharynx and atypical early symptoms of NPC, majority (~70%) of patients diagnosed with NPC have already reached an advanced stage ⁽²⁾. Standard concurrent chemoradiation therapy (CCRT) in locally advanced disease is routinely used to manage the disease and seem to be satisfied with high overall survival. Currently, this is achieved monitoring change in tumor size by using computed tomography (CT) or magnetic resonance imaging (MRI). Unfortunately, this assessment monitors a relatively late event because anatomical change usually occurs later than functional changes, and these assessments are usually undertaken halfway through the course of treatment. So, biomarkers that can provide an early indication of response are essentially required.

Diffusion-weighted imaging (DWI) is an MRI technique which provides functional information of tissue by detecting microscopic motion of water molecules. Conventionally, the change of apparent diffusion coefficient (ADC) derived from DWI was used as an imaging biomarker for treatment response prediction in cancers. However, it is based on whole-tumor analysis which did not reflect heterogeneity within the tumor. To overcome this limitation, a new method called parametric response map (PRM) analysis is proposed to evaluate response by quantifying voxel-wise changes in ADC.

In PRM analysis, individual voxels were labeled into three categories based on the change in ADC at mid-treatment with respect to pre-treatment. Specifically, ADC maps which were derived from acquired diffusion MRI data at pre-treatment and mid-treatment are co-registered. Voxel-by-voxel subtraction between co-registered mid- and pre-treatment ADC maps is performed to create a map of ADC change. Individual voxels within tumor in the co-registered pre-treatment ADC map are classified into three categories based on the change in ADC or ΔADC . Red voxels represent areas where ΔADC is beyond a pre-defined threshold. Green voxels represent no change in ADC. Blue voxels represent areas where ΔADC is below a pre-defined threshold. After compute the voxel of three categories, therefore we got PRM value (PRM₊, PRM₋, PRM₀, respectively). However, only the volume of tumor with a significant increase in ADC (PRM₊) was directly correlated with favorable clinical outcome. This PRM analysis can also be presented using a scatter plot and percentages assigned to the three categories, allowing quantitative assessment of overall changes in tumor ADC values.

In this research project, we used PRM₊ analysis on ADC from DWI as an imaging biomarker to predict treatment response in NPC patients. We evaluated its performance as compared with the conventional methods using change in tumor size and change in ADC values between pre-treatment and mid-treatment scans.

1.2 Research questions

1.2.1 Primary question

Is the imaging biomarker based on PRM (PRM₊) in complete responders different from that in partial responders?

1.2.2 Secondary question

What is the performance level of PRM₊, volume change, and ADC change in predicting treatment outcome of nasopharyngeal carcinoma?

1.3 Research objective

1.3.1 Primary objective

To compare PRM₊ analysis between complete responders and partial responders.

1.3.2 Secondary objective

To compare the performance of predicting treatment outcome of PRM₊, volume change and ADC change in nasopharyngeal carcinoma.

1.4 Significance and impact of the work

Chemoradiation therapy is the common types of cancer treatment which work by destroying these fast-growing cells. However, it can be damaged along with normal cell and cancer cells causing adverse reactions or side effects such as nausea, fatigue, and increased change of infection. So, imaging biomarker were used to obtain the remarkable clinical benefit for patients and improve entire health care system.

The objective of this study was to investigate the use of PRM analysis on ADC from DWI as an imaging biomarker for early predict response of standard concurrent chemoradiation therapy of nasopharyngeal carcinoma.

1.5 Definition

Apparent diffusion coefficient (ADC)

A measure of the magnitude of diffusion of water molecule within the tissue, which is calculated using MRI with 2 b- value on DWI sequence. The unit is mm²/s.

Concurrent chemoradiation therapy (CCRT)	The combined use of chemotherapy delivered concurrently with radiation in cancer treatment. It is for patients with the local region advanced stage of NPC.
Tumor heterogeneity	The differences between tumors of the same type in different patients, and between cancer cells within a tumor. It can show distinct morphological and phenotypic profiles.
Parametric response map (PRM)	A voxel-based image-analysis technique for the change of diffusion of water by MRI scan. It provides a color map and gives treatment response to the disease.
PRM+	The percentage of voxels with increased ADC values more than a pre-defined threshold with respect to total voxels within the tumor ROI (displayed in red voxel).
Voxel	A unit of image information that defines a point in three-dimensional space, regular matrix.

CHAPTER II

THEORY AND RELATED LITERATURE

2.1 Theory

2.1.1 Magnetic resonance imaging (MRI)

MRI is a non-ionizing technique that uses a strong magnetic field (B_0) and radio frequency (RF) to produce high-resolution anatomical information with excellent soft-tissue contrast. MRI is providing information different from other imaging modalities because it can characterize tissues by using their physical and biochemical properties such as water, iron, fat, and blood. It can be used to examine almost any part of the body. Moreover, the main advantage for the MRI is diagnostic, MRI can diagnose in many different types of diseases such as structural disease, organ dysfunction, and cancer.

In addition, functional MRI (fMRI) is advanced MRI technique used to obtain tumor biology by providing quantitative functional information such as diffusion weighted imaging (DWI), dynamic contrast enhanced (DCE), and perfusion-weighted imaging (PWI). Nowadays fMRI is more popular because it is non-invasive which some sequence does not require the injection of a radioisotope to see the function information such as blood vessel and get good spatial resolution. Increasingly, fMRI is being used as a biomarker for disease to monitor therapy, or for studying pharmacological efficacy⁽³⁾. Moreover, in this study was focus on DWI technique.

2.1.1.1 Diffusion-weighted imaging (DWI)

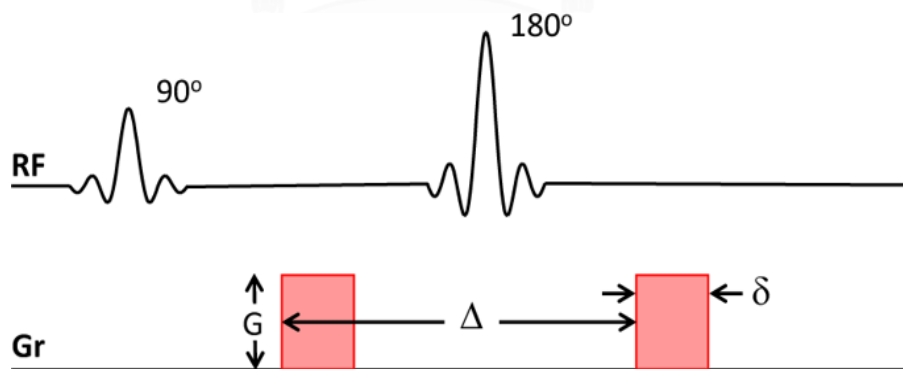


Figure 1 Simplified MRI spin echo pulse sequences of DWI⁽⁴⁾.

DWI is a powerful MRI technique which probes abnormalities of tissue structure by detecting microscopic changes in water molecules due to thermal Brownian motion within a voxel of tissue. In clinical oncology, highly cellular tissues or cellular swelling exhibit lower diffusion coefficients because cells have dense and restriction diffusion the water movement that it is useful in

tumor characterization and classify stroke. DWI is typically performed using an echo-planar imaging (EPI) technique which is a fast magnetic resonance imaging technique capable of acquiring an entire MR image in only a fraction of a second. It was achieved all frequency-encoding and phase-encoding by rapidly oscillating read-out gradient. EPI offers major advantages over conventional MR imaging, including reduced imaging time, decreased motion artifact, and the ability to image rapid physiologic processes. Moreover, the use of EPI has already resulted in significant advances in clinical diagnosis, and scientific investigation. Nevertheless, it also has the disadvantages that are low signal to noise ratio (SNR), and some imaging artifact such as chemical shift artifacts; susceptibility artifacts; ghosting; and geometric distortion ⁽⁵⁾. So, the periodically rotated overlapping parallel lines with enhanced reconstruction (PROPELLER) technique was developed by Pipe in the late 1990s for artifact reduction and overall image quality improvement ⁽⁶⁾.

To generate DWI, it must apply two diffusion gradients between the 180° RF pulse which can be added to conventional MR sequences as can be seen in Fig.1. The first diffusion gradient introduces phase shift to the protons depending on their positions while another diffusion gradient is applied in the same magnitude but with opposite direction to rephase the spins.

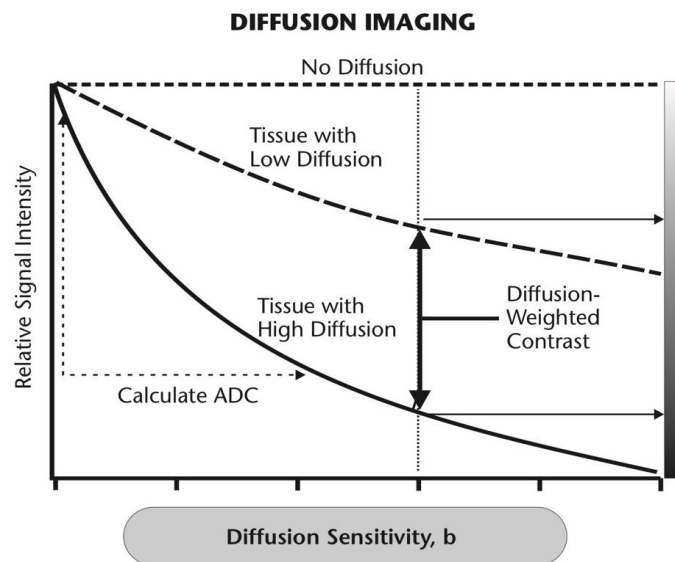


Figure 2 The relationship of relative signal intensity of the regions of interest in the diffusion-weighted image (Y-axis) and diffusion sensitivity or b-value (X-axis) ⁽⁷⁾.

If there are movements of protons, the second gradient will not be able to completely undo the changes. As a result, there will be shown signal attenuation given by:

$$S_b = S_0 e^{-bD},$$

where S_b is the diffusion-weighted signal, S_0 is the signal without diffusion weighting (i.e. T2-weighted image), the degree of attenuation is defined by the product of b-value, and D is a constant which is the apparent diffusion coefficient (ADC) value. ADC represent averages of the entire voxel and of each direction of diffusion (units: mm^2/s).

The diffusion-weighting factor (b-value) is a value that includes all gradient effects. The value is given in units of s/mm^2 . It can determine by Stejskal-Tanner equation who derived in signal attenuation due to the application of the pulse gradient related to the amount of diffusion ⁽⁸⁾. The b-value is given by

$$b = \gamma^2 G^2 \delta^2 \left(\Delta - \frac{\delta}{3} \right)$$

where γ is the gyromagnetic ratio (42.58 MHz/T for Hydrogen atom), G is the strength of the diffusion gradients, δ is the duration of the gradient which is equal and opposite in two gradients, and Δ is the time interval between these gradients. In clinical practice, b-values of 0 – 1500 s/mm^2 are applied.

For the images analysis, to evaluate diffusion-weighted MRI there are two general categories: qualitative and quantitative. The image contrast of DWI base with T2* effects (b-value equal 0), and it can be adjusted by the range of b-value. As higher b-value, diffusion signal has an increase as shown in Fig.2. In case of movement in photon, no net movement of protons in between the two gradient applications, both the gradient effects cancel out each other and there will be no signal attenuation and it will appear brighter in the image. If proton have diffusion motion, there will not be complete rephrasing and will be attenuation in signal resulting in darker regions on the images.

In clinically, the ADC image leading to an inverted scale similar to the DWI but eliminating T2 shine-through effects. For many abnormalities, it not only restricts only the diffusion but are bright on T2. So, it can actually use advantage of the T2 shine-through effect to confirm true diffusion restriction of lesion on the ADC image as shown in Fig.3.

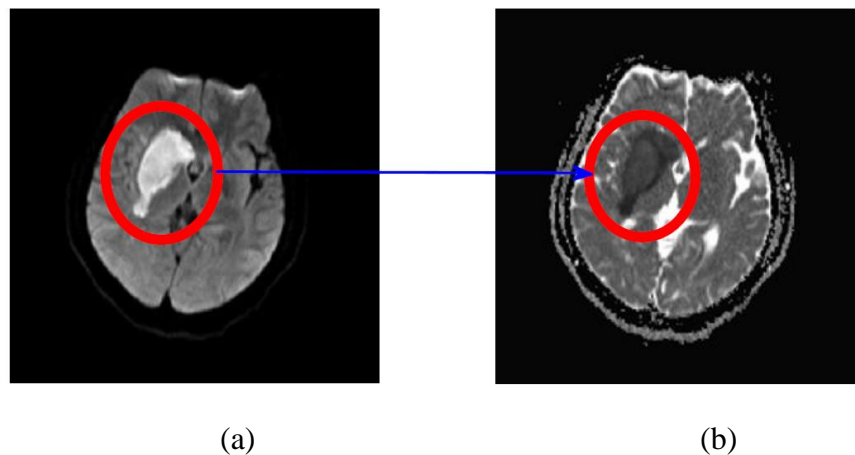


Figure 3 The DWI (a) and ADC (b) image of MRI brain. The red circle is highlighting abnormality (a stroke region) in the brain ⁽⁹⁾.

2.1.2 Biomarker

Biomarker, which is short form of biological markers, it is a measurable indicator of a biological state. It have been defined by Hulka and colleagues ⁽¹⁰⁾. Biomarkers are useful in a number of ways including predicting and monitoring disease, evaluating the therapeutic effective for a cancer type, and evaluating the recurrence of cancer ⁽¹¹⁾.

Biomarkers can be classified based on parameters and characteristics, such as imaging biomarkers; base on imaging machine such as CT, PET, and MRI, or molecular biomarkers; base on blood and body fluids, and biopsy biomarkers. In this study, the researcher was focus on imaging biomarker by MRI.

Imaging biomarker is a feature of an image relevant to treatment efficiency of a patient. The advantage of imaging biomarkers by MRI is having a high spatial resolution, high sensitivity, and superior soft-tissue contrast for structural or functional imaging. A number of MRI in imaging biomarkers are already established in clinical practice for oncological assessments such as BI-RADS (Breast Imaging Reporting and Data System) for the diagnosis of breast ⁽¹²⁾, transfer constant (K_{trans}) from dynamic contrast enhanced (DCE) imaging, and ADC from DWI. Characteristics of a good biomarker following features: sensitive, specific and biologically relevant, robust, quantifiable and reproducible, and cost effective ⁽¹³⁾. For effective and early biomarkers can avoid inefficient treatments of individual patients and improve the entire health care system.

2.1.3 Parametric Response Map (PRM)

PRM is a voxel-based analysis technique spatially registered the pretreatment ADC map to a mid-treatment ADC map to provide for quantification of diffusion changes on the voxel level for predicting the effect of treatment. PRM of ADC, it is widely accepted that tumor ADC values increase following a successful treatment which reflects a reduction in cellular density and in barriers to water motion. In lesion, increases in ADC would reflect an increase in the mobility of water, or a decrease in a lesion size shown in normal cells. On the contrary, decreases in ADC reflect a decrease in free extracellular water, either through an increase in total cellular size, as can be seen with tumor progression⁽¹⁴⁾. The efficacy of PRM was also studied by Baer A.H., *et al.*⁽¹⁵⁾ and Drisis S., *et al.*⁽¹⁶⁾. For treatment response prediction in oncology, change of ADC (ΔADC) in a lesion can be used as a biomarker which is computed by

$$\Delta ADC_M = ADC_M - ADC_P,$$

where ADC_P is pre-treatment lesion ADC value and ADC_M is lesion ADC value at day N after the initiation of therapy or the so-called mid-treatment ADC value. The higher ADC change indicates higher chance of better treatment outcome.

The changes of ADC (ΔADC) in individual voxels within tumor is necessary to classify voxels into three categories as increasing, decreasing, or unchanged. Red voxels represent areas where ΔADC is beyond a pre-defined threshold. Green voxels represent no change in ADC. Blue voxels represent areas where ΔADC is below a pre-defined threshold.

2.1.4 Image processing

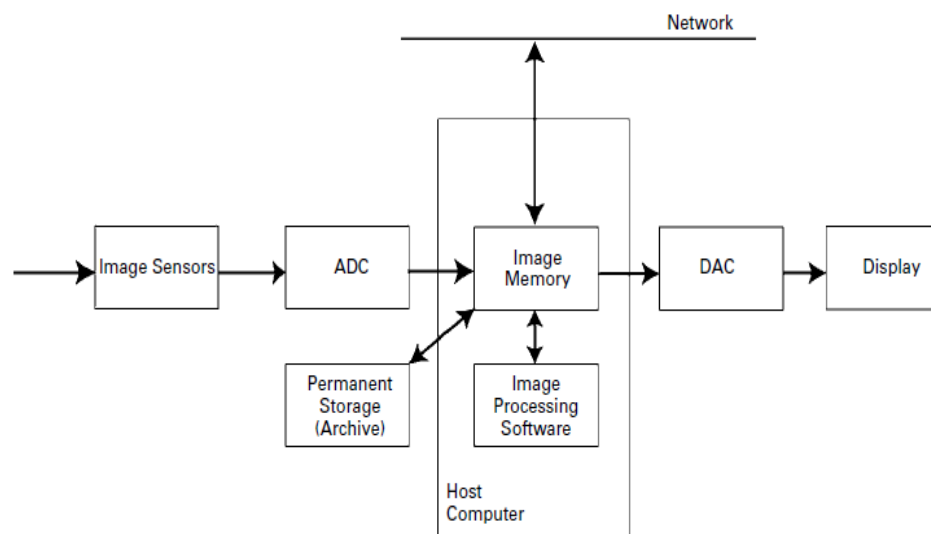


Figure 4 Image processing system⁽¹⁷⁾.

Medical imaging is the process of producing visible images of the inner structures of the body. The image will classify into two groups analog and digital images. Only digital image can be presented by a discrete value that can make storage and processing in the computer. It has many benefits such as elasticity, adaptability, data storing, and communication. The common standard of medical image for managing, and storing is Digital Imaging and Communications in Medicine (DICOM). It can keep both of receiving image and patient data.

The digital image processing system is collection of equipment and software as shown in Fig.4. It starts with acquire digital image (discrete) from the receptor. If the detected image is analog (continuous), it will need to be modify by analog-to-digital converter (ADC) after that process and display the image on monitor. This requires the production of an analog signal by a digital-to-analog converter (DAC) ⁽¹⁷⁾.

The medical imaging processing refers to handling images by using the computer. Applications of digital image processing includes has many applications in the medical field such as: segmentation, registration, and transformation ⁽¹⁸⁾.

2.1.4.1 Image segmentation

Image segmentation is a highly important tool in image analysis that it is a technique of the identifying of region in image. The basic aim of this segregation is to make the images easy to analyze and interpret with preserving the quality. The application include; defined region of interest (ROI), measurement of area and volume in medical image datasets, definition of target areas under considering, and definition organs-at-risk in radiotherapy ⁽¹⁹⁾.

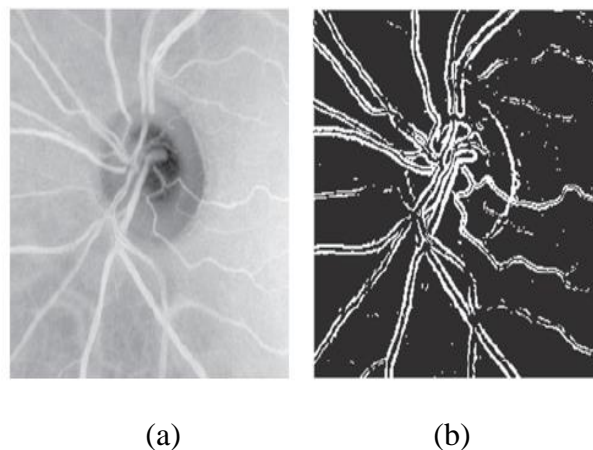


Figure 5 (a) Original image of retinal vessel, (b) image after registration in thresholding technique ⁽²⁰⁾.

Classification of the ROI of an image can be performed using a manual or automatic. The simple of manual way is draw boundary over the region in each baring slide. For automatic segmentation, there are many different

techniques had been proposed to detect ROI; for instance, thresholding (Fig.5), region growing, and snake (active contour). The thresholding is the straight forward approach which select an ROI by define an intensity threshold. This method is useful for establishing the borders of solid objects in a dark background. In terms of region growing, it is semi-automatic segmentation which refines the thresholding and adds a requirement that pixel should be connected. However, it has limitation that the result depends on the choice of initial parameters.

2.1.4.2 Image registration

Image processing is the process of transforming one image into another coordinate image. This process involves determined one image as the reference image (fixed image), and using suitable geometric transformations to the other images (moving image) so that they align with the reference. The registration can categorize by the type of image data or form of they operate.

- Intramodal and Intermodal registration

Intramodal registration is the registering image that from the same modality in different time and/or different position two; an example is CT_{t1} -to- CT_{t2} registration of volumes acquired at different times. This procedure is helpful when doing time series evaluation, for instance when tracking the effect of chemo- or radiation therapy on tumor growth.

As for intermodal registration is registering image data from different imaging modality into the same coordinate system; an example is MR-to-PET, MR-to-CT (see Fig.6).

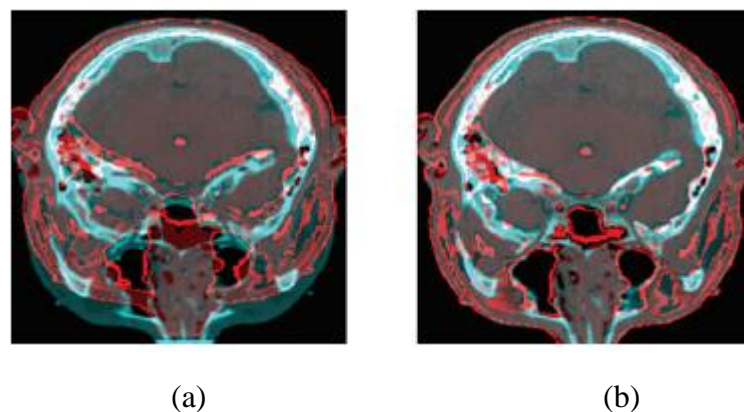


Figure 6 Intermodal registration CT (cyan color) and transformed MRI (red color). (a) unregistered image, (b) registered image ⁽²¹⁾.

- Rigid and Non-rigid registration

Rigid registration uses a simple transform and uniformly applied. The transformation models include linear transformations, which include rotation, scaling, translation, and other affine transforms; thus, they cannot model local geometric differences between images. The parameter of translation and rotation in 2D is 3 parameters (2 for translation, 1 for rotation), and in 3D is 6 parameters (3 for translation, 3 for rotation).

Non-rigid registration (Deformable registration), it allows one image to be deformed to match another in order to account for the non-linear local anatomic variations that exist between the images. The transformation models include allow 'elastic' or 'nonrigid' transformations include radial basis functions, physical continuum models, and large deformation models.

2.1.5 Nasopharyngeal carcinoma (NPC)

NPC is one of the major types of head and neck cancer which develops in nasopharynx in a small site bordered by the nasal cavity, the posterior wall continuous with the posterior wall of the oropharynx, the body of the sphenoid and basilar part of the occipital bone, and the soft palate. About 90% of malignant tumors are squamous cell carcinoma (SCC) and 10% are the other type⁽²²⁾. Due to anatomic locations of the nasopharynx and early symptoms of NPC patients, majority of patients (~70%) are diagnosed with advance stage disease (stage III to IV)⁽²⁾.

2.1.5.1 Causes of nasopharyngeal carcinoma

No one is sure what exactly causes nasopharyngeal carcinoma. It may like other cancers, the risk of developing NPC includes: Epstein-Barr virus (EBV), the use of alcohol and tobacco. Other risk factors are age, gender, family history, environmental exposure, and eating habits. It is commonly diagnosed between 40 to 60 years. Males are more commonly affected, with the ratio of 2:1 (Male: Female)⁽²⁰⁾. The risk of NPC is endemic in Asian, particularly those from southern China and southeast Asia.

2.1.5.2 Signs and symptoms of nasopharyngeal carcinoma

It is often difficult to diagnose NPC in the early stages because of the tumor located. In many cases, NPC gets large before patients knew. In rare cases, the cancer may not be detected until a patient has severe bone pain (in the legs or spine), and diagnostic tests show a cancer. The sign and symptoms of NPC patients at presentation include a swollen lymph node at the neck; which is the most common symptom, hearing loss, bleeding from nose or mouth, blurring vision, and headache.

2.1.5.3 Radiological staging

The radiological test is essential in clinical staging of NPC as it used to identify the tumor location and lymph node. For many procedures, MRI is a diagnostic procedure that uses a magnet, RF waves, and a computer to generate a picture inside the body. It more sensitive than CT. According to FDG-Positron emission tomography (PET) is the best procedure to find metastasis and recurrent NPC. However, Use the combination of FDG-PET and MRI is more accurate for tumor restaging (overall accurate 92.1%)⁽²³⁾.

All patients' NPC staging refers to TNM staging system of malignant tumors of the nasopharynx follow the 8th edition of the American Joint Committee on Cancer (AJCC). TNM staging is a diagnostic test to find out the cancer stage, prognostic stage groups and decide the treatment of the patient. For more details of each part of the TNM staging, where tumor (T) is how large of the primary tumor and where it is located, node (N) has the tumor spread to the lymph nodes, and metastasis (M) has cancer spared to other organs of the body. So, the cancer stage is combining of the T, N, M. In more information, see Table 1⁽²⁴⁾.

2.1.5.4 Treatment

NPC have significantly differences from other head and neck cancers in its occurrence, causes, and treatment strategies. There are different types of treatment for NPC patient such as; radiation therapy, chemotherapy, and surgery. However, Radiation therapy has played the most important and central role in the definitive therapy for the patients because NPC is highly sensitive to radiation therapy. Moreover, treatment for NPC may cause many side effects such as: tooth decay, redness of the skin in the treated area, dry mouth from damage to salivary glands, hair loss, nausea, fatigue, pain or difficulty swallowing, and loss of appetite because of changes in a person's sense of taste.

In the high stage cancer, the combination way, which is most recent and most popularized nowadays, is the standard concurrent chemoradiation therapy (CCRT) followed by adjuvant chemotherapy (AC) in patients with locally advanced and non-metastatic stage NPC. The report from Blanchard P. and others founded that CCRT follow by AC had a significantly for 5-year overall survival benefit better than radiotherapy alone (67% vs. 37%, respectively)⁽²⁵⁾.

Currently, this is achieved by monitoring changes in tumor size by using CT and/or MRI. Unfortunately, this assessment monitors a relatively late event because functional changes occur prior to alterations in size and tumor size assessments are usually undertaken halfway through a course of treatment. So, it is increasingly important to predict early response to CCRT in order to identify patients who can respond to treatment while avoiding unnecessary treatment. Therefore, biomarkers that can provide an earlier indication of response are essentially required.

Table 1 TNM staging of cancer by AJCC

Stage	Stage grouping	Stage description
0	Tis, N0, M0	The tumor is located inside of the nasopharynx, with no spread to lymph nodes and no distant metastasis
I	T1, N0, M0	The tumor is in the nasopharynx. It might in oropharynx and/or nasal cavity, with no spread to lymph nodes and no distant metastasis
II	T1 (or T0), N1, M0 OR T2, N0 or N1, M0	The tumor is in the nasopharynx it might in oropharynx and/or nasal cavity. Or, no tumor is seen in the nasopharynx, but it founds in lymph nodes in the neck and EBV positive, but no metastasis OR This stage may also describe a tumor that has beyond the nasopharynx but has not spread to lymph nodes or metastasis. It may also describe a tumor that has spread to lymph nodes but no metastasis
III	T1 (or T0, T2), N2, M0 OR T3, N0 to N2, M0	A noninvasive or invasive tumor that has spread to lymph nodes on both sides of the neck above the triangular area but no metastasis OR This stage may also describe a larger tumor with or without lymph node involvement and no metastasis
IVA	T4, N0 to N2, M0 OR Any T, N3, M0	This describes any invasive tumor with either no lymph node involvement or spread to only a single same-sided lymph node but no metastasis (T4, N0 or N1, M0). It is also used for any invasive tumor with more significant lymph node involvement but no metastasis (T4, N2, M0). OR It also describes any tumor with extensive lymph node involvement but no metastasis.
IVB	Any T, Any N, M1	This describes any tumor when there is evidence of metastasis
	Recurrent	cancer that has come back after treatment. If the cancer does return, there will repeat the tests and determine the staging.

Abbreviations: Tis = carcinoma in situ

2.2 Review of related literatures

Cui Y., Zhang X. P., Sun Y. S., Tang L. & Shen L. (2008) ⁽²⁶⁾ reported ability of Δ ADC as an imaging biomarker in 23 patients with colorectal and gastric hepatic metastases in chemotherapy with a total of 87 lesions. Imaging were performed before and 3, 7 and 42 days after starting of chemotherapy. The mean ADC of patients measured by using DWI imaging. The results showed that Δ ADC after treatment in days 3 and 7 seems to be a promising tool for helping predict and monitor the early response to chemotherapy of hepatic metastases from colorectal and gastric carcinoma.

Like **Harry, V. N., et al. (2008)** ⁽²⁷⁾, who studied 20 patients with advanced cervical cancer and chemoradiation treatment. Imaging and clinical examinations were performed before chemotherapy started, at 2 weeks after the start and at the end of therapy. From the results, ADC values after 2 weeks of therapy showed a significant correlation with eventual MRI response and clinical response. They further concluded that DWI has the potential to provide a biomarker of treatment response in advanced cervical cancers.

An extensive review of literature has shown that using an early increase ADC may be a predictor of response to treatment. These are two of many papers that have been evaluated ADC as a response biomarker in a number of tumor types across different therapies ⁽¹³⁾.

Even though lesion ADC change may be a useful predictor for treatment response, a recent study reported that change of ADC in lesion had a limitation because it was based on whole-tumor analysis which did not reflect heterogeneity within the tumor ⁽²⁸⁾. To overcome this limitation, a new method called parametric response map (PRM) was proposed to evaluate response over time by quantifying voxel-wise changes in ADC ⁽²⁹⁾.

Reischauer C, Froehlich JM, Koh DM, Graf N, Padevit C, et al. (2014) ⁽³⁰⁾ compared Δ ADC and PRM analysis in 9 patients diagnosed with advanced non-small cell lung cancer with 13 lung tumors total and showed that this approach may prove to be more sensitive to changes resulting from therapy compared with mean ADC changes averaged over entire lesions as it accounts for heterogeneous changes that occur within each tumor with treatment. In previously published results by Yabuuchi *et al.* ⁽³¹⁾ shown that an increase in the mean ADC at three to 4 weeks compared with pre-treatment values could predict good response in patients with non-small cell lung cancer. However, this study has shown that PRM potentially is observed as early as 1 week after starting treatment. It can conclude that this paper used the new method PRM that more accuracy for evaluation of cancer treatment response.

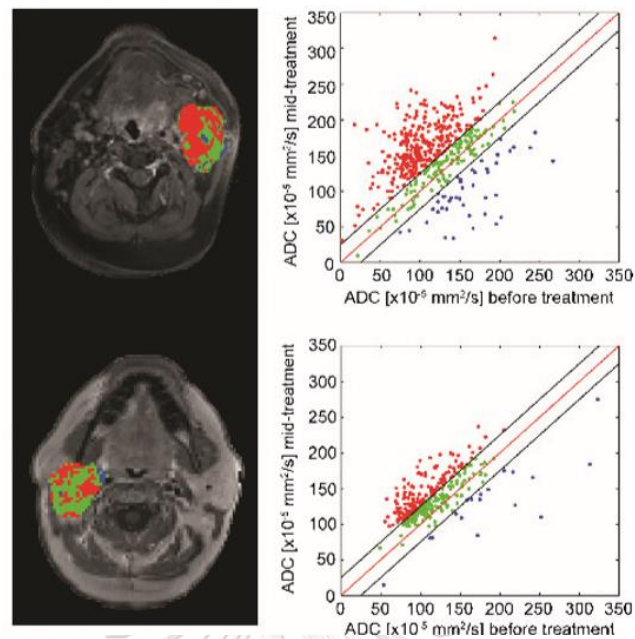


Figure 7 Representative patients with HNSCC stratified by PRM as a responder (top row) and a non-responder (bottom row) at the time of analysis. The scatter plots show the distribution of changes in PRM throughout the entire volume of interest. Voxels with significantly increasing, decreasing, or unchanged are coded as red, blue, and green dots, respectively ⁽³²⁾.

Galbán, et al. (2009) ⁽³²⁾ evaluated the feasibility of monitoring treatment response to chemoradiation therapy in 15 patients with head and neck squamous cell carcinoma (HNSCC) AJCC stage III/IV disease based on the recommendation of a multidisciplinary head and neck tumor treatment use nonsurgical organ preservation therapy (NSOPT) concurrent radiation and chemotherapy. PRM analysis was performed on ADC changes before therapy and 3 weeks after the therapy started. The PRM Analysis will classify treatment response by three categories base on the change in ADC voxel where PRM_+ is increased ADC shown in red voxels, PRM_0 is unchanged ADC shown in green voxels and PRM_- is decreased ADC shown in blue voxels (shown in Fig.7). This study found that responder and non-responder of patient had negligible differences in percentage change in mean ADC. Nevertheless, percentage change in Tumor volume and PRM_+ were significantly associated with disease control ($p < .05$). Further evaluation of the predictive value was performed using an ROC curve analysis correlated with clinical progression. The percentage changes in tumor volume and mean ADC were not significantly associated with clinical progression shown AUC equal 0.758, $p = 0.06$ whereas PRM_+ (AUC = 0.825, $p = .02$) as shown in Fig.8

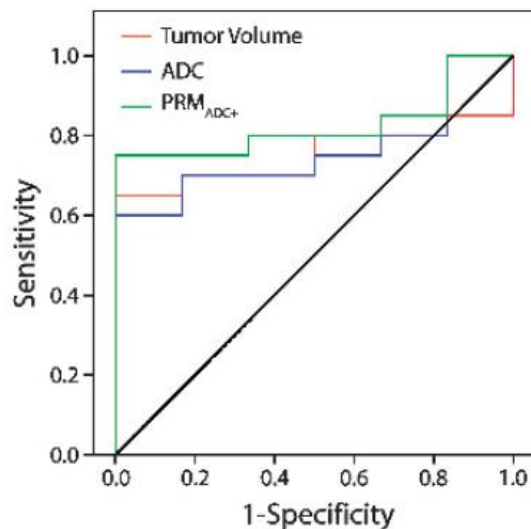


Figure 8 Receiver operating characteristic curve of treatment response in percentage change in tumor volume (red), mean ADC values (blue) and PRM analysis which exhibited a significant increase in ADC (green).

It can be concluded that the percentage changes in tumor volume with significantly increased ADC values as assessed by PRM₊ at 3 weeks in to a course of chemoradiation therapy were predictive of disease control at 6 months in head and neck cancer patients. However, their study had a limitation that there is needed to be validated with more patient's data. Of 15 head and neck cancer patients, only 3 were found to have progressive disease 6 months after treatment. In fact, preclinical models have shown that the greatest ability for diffusion MRI to predict response was before a significant change in tumor volume had occurred. So, multiple time-point evaluations are needed to measure changes in diffusion.

Base on the aforementioned studied, it could be concluded that the diffusion MRI, when assessed by PRM, has the potential to predicted treatment response in a number of tumor types across different therapies. The volume of the tumor with a significant increase in ADC (PRM₊) was directly correlated with favorable clinical outcome and there was no association between the volume of the tumor with decreasing ADC (PRM₋) and clinical progression⁽³³⁾.

Table 2 Overview of 4 literatures

Study	Biomarker, scan time point	DWI Scanning protocol	Tumor Type	Sample	Treatment	Conclusions
Cui Y., Zhang X. P., Sun Y. S., Tang L. & Shen L. (2008)	Δ ADC	1.5 T; (b = 0, 800 s/mm ²)	Colorectal and gastric hepatic metastases	23 (87 lesions)	Chemotherapy	Δ ADC can be used in a number of tumor types across different therapies
	Δ ADC	1.5 T; (b = 0, 1000 s/mm ²)	Cervical cancer classification IB to IVB	20	Radiation and Chemotherapy	
Reischauer C, Froehlich JM, Koh DM, Graf N, Padevit C, <i>et al.</i> (2014)	% Δ ADC	1.5T; (b = 100, 600, 800 s/mm ²)	Advanced non-small cell lung cancer stage III/IV	9 (13 lesions)	Chemotherapy	The PRM ₊ analysis is more accurate for evaluation of cancer treatment response than ADC analysis
	PRM ₊					
Galbán, <i>et al.</i> (2009)	PRM ₊	3 T; (b = 0, 1000 s/mm ²)	Head and neck cancer with squamous cell carcinoma	15	Radiation and Chemotherapy	PRM analysis is nearly biomarker for monitoring therapeutic efficacy in patients with head and neck cancer

Abbreviations: ADC, apparent diffusion coefficient; PRM, parametric response map; T, tesla.

CHAPTER III

RESEARCH METHODOLOGY

3.1 Research design

This research was designed as a diagnostic test in the type of retrospective-prospective study to a patient with nasopharyngeal carcinoma.

3.2 Research design model

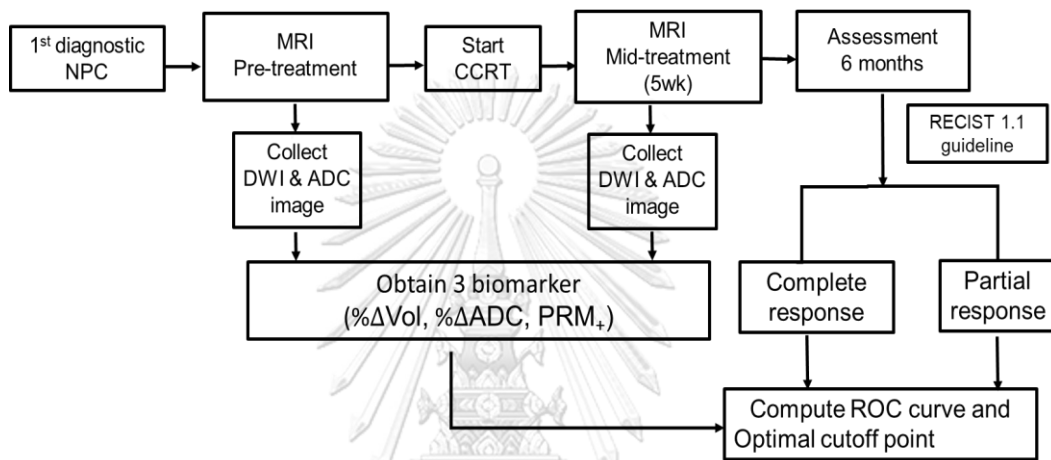


Figure 9 Research design

3.3 Conceptual framework

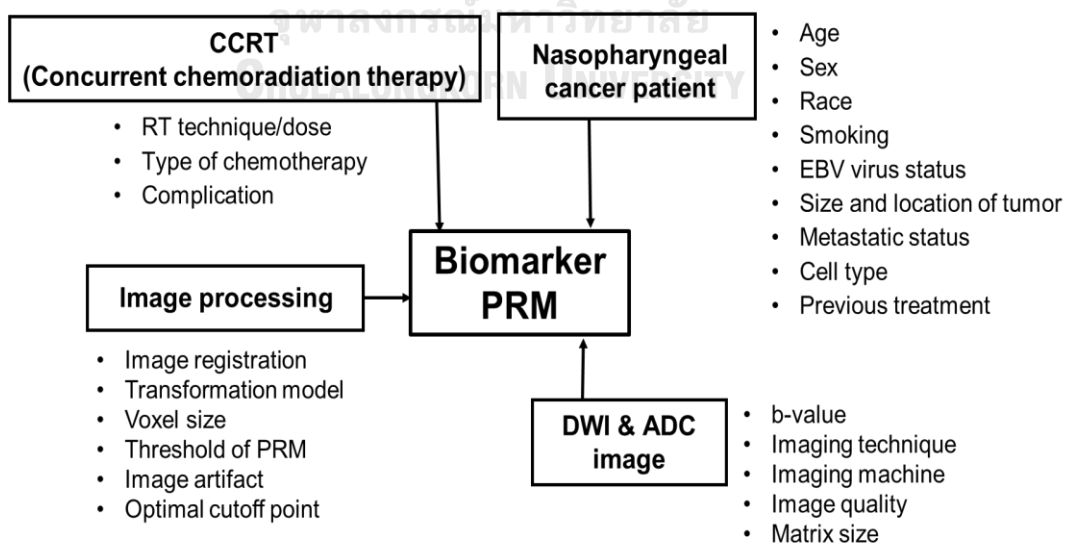


Figure 10 Conceptual framework

3.4 Key Word

Diffusion Weighted Imaging, Apparent Diffusion Coefficient, Parametric Response Map, Nasopharyngeal carcinoma.

3.5 The sample

3.5.1 Target population

All MRI with DWI image data set of nasopharyngeal carcinoma patients who treated and followed up at division of radiation oncology, King Chulalongkorn Memorial Hospital (KCMH).

3.5.2 Sample population

The MRI with DWI images dataset at pre-treatment and mid-treatment of nasopharyngeal carcinoma patients who treated and followed up at division of radiation oncology, KCMH and met the eligible criteria.

3.5.3 Eligible criteria

3.5.3.1 *The inclusion criteria*

Patients with the first diagnostic with nasopharyngeal carcinoma with proved pathology complete staging with bone scan, ultrasonography (US), CT or MRI, EBV viral load, with or without PET/CT scan at KCMH. All patient will be evaluated with MRI DWI for radiation treatment planning before treatment verification and treatment delivery following radiation treatment process.

3.5.3.2 *The exclusion criteria*

Patients who lost follow up or treatment within the first 6 months. The researcher did not include patients who were undergoing concurrent chemotherapy and radiation therapy, or whose data have registration mismatch of the tumor at ADC image and contraindications to MRI.

3.5.4 Sample size determination.

The sample size was determined according to the formula

- Primary objective

$$n = \frac{2\sigma^2(Z_{\alpha/2} + Z_{\beta})^2}{d^2}$$

where

$$Z_{\alpha/2} = 1.96 \text{ (95\% Confidence level; } \alpha = 0.05)$$

$$Z_{\beta} = 0.84 \text{ (Power of 80\%)}$$

$$\sigma^2 = 49 \text{ (The population variance of patient-response patient in PRM) }^{(32)}$$

$$d = 18 \text{ (The hypothesis difference) }^{(32)}$$

$$\therefore n = 3 \text{ (Partial-response patient)}$$

According to data statistic from Galbán, *et al* ⁽³²⁾, the ratio of patient with complete-response and partial-response $\approx 10:3$. Thus, number of patient with partial-response are 3 and complete-response are 12.

So, we will use at least 15 patient datasets.

- Secondary objective

Comparing two independent groups for continuous data by Mann–Whitney U test.

$$n = \frac{2.09 (z_{1-\alpha/2} + z_{1-\beta})^2}{\Delta^2},$$

where

$$(Z_{1-\alpha/2} + Z_{1-\beta})^2 = 7.849 \text{ (} \alpha = 0.05, 1 - \beta = 0.80)$$

$$\Delta = 0.2 \text{ (The participated effect size for “large effect”) }^{(34)}$$

$$n = 25.631$$

$$= 26$$

Therefore, the eventual sample size was at least 26 patient datasets.

3.6 Materials

3.6.1 Magnetic resonance imaging simulator



Figure 11 MRI Simulator GE Medical systems at KCMH

Imaging Acquisition of scans was done with the MRI system with 1.5 Tesla at Division of Radiation oncology, KCMH acquired in a patient with the six-channel surface coil as shown in Fig.11. The system is manufactured by GE Medical systems (Signa HDxt, GE Medical systems, Chicago, United States).

3.6.2 3D Slicer software

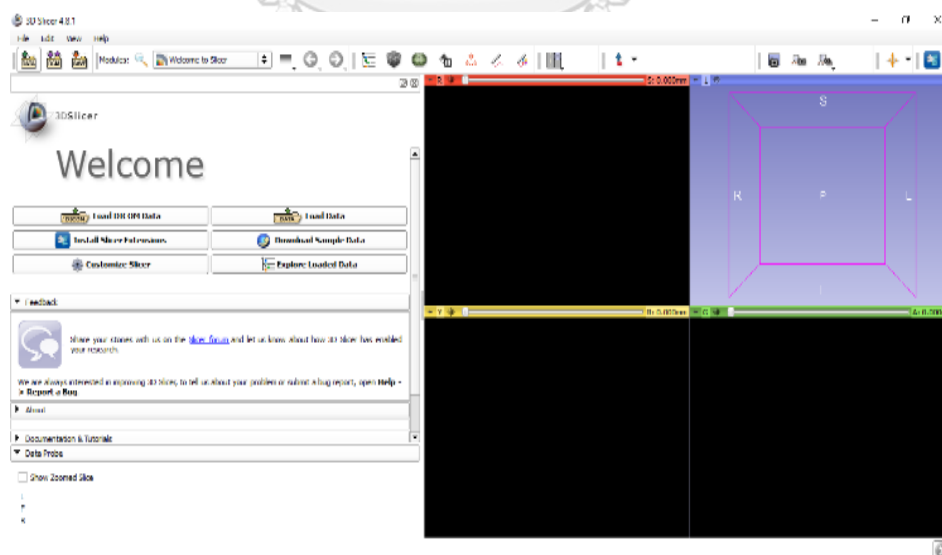


Figure 12 3D Slicer software

The 3D slicer software is an open source software for medical image informatics, image processing, and three-dimensional visualization by the National Institutes of Health (NIH) and a worldwide developer community (BSD License). It provides a platform for a variety of applications through a community-development model. The resulting system has been used for research in both basic biomedical and clinically applied settings. This study used 3D Slicer version 4.8.1 as in Fig.12 for a region of interest (ROI) drawing and reading/writing image into other formats; i.e. .nrrd, .raw, and .tiff⁽³⁵⁾.

3.6.3 Image J software

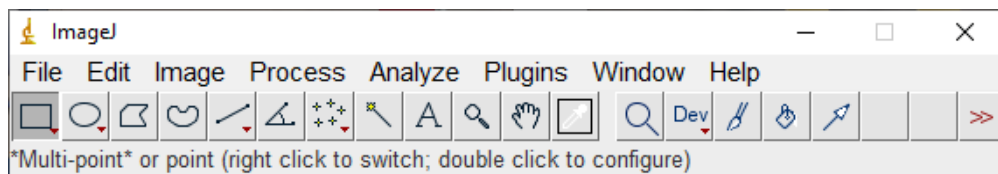


Figure 13 Image J software

Image J is a public image processing and analysis program in Java inspired by National Institutes of Health (NIH) and the Laboratory for Optical and Computational Instrumentation (LOCI, University of Wisconsin). Image J is available for Microsoft Windows, the classic Mac OS, Linux, and the Sharp Zaurus PDA. ImageJ can read, display, edit, analyze, process, and save images in many format file (see Fig.13)⁽³⁶⁾.

3.6.4 MATLAB software

MATLAB (MATrix LABoratory) is a high level technical computing language developed by Math Works (The Mathworks, Inc., Natick, Massachusetts), Version R2018a. It can integrate computation, visualization, and programming in an easy-to-use environment including algorithm development, modeling, simulation, data analysis, exploration, and visualization.

3.7 Methods

3.7.1 Patient data collection

The patient's data set were extracted from diagnostic and radiation oncology department in synapse (PACS) system. The data set include images, and the clinical characteristics of patient such as age, gender, hospital number, acquisition date, and staging were collected in the case record form in APPENDIX B.

The imaging collected from MRI simulator 1.5 T with routine MRI simulation protocol except for diffusion-weighted sequence. For each patient, MRI study was performed at 2-time point before treatment and five-weeks after initiation of chemoradiation therapy (CCRT). DWI data were acquired in the axial plane, non-echo-

planar imaging (EPI) series with PROPELLER technique. The field of view covers the entire primary tumor volume and interested organ (TR/TE 5000 ms /79.806 ms, b factor 0 and 800 sec/mm², receiver bandwidth 650.78 Hz/pixel, slice thickness 5 mm, gap 5 mm, Echo train length 16, and FOV 260 cm²) in pre-treatment and mid-treatment. The clinical ADC, using all 2 b-values, was used in this analysis. Display matrix size was 256 x 256 pixels in Digital Imaging and Communications in Medicine (DICOM) format files as in Fig.14.

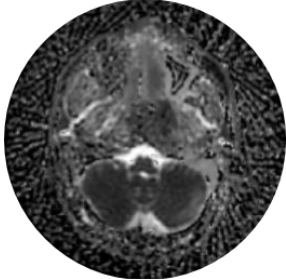
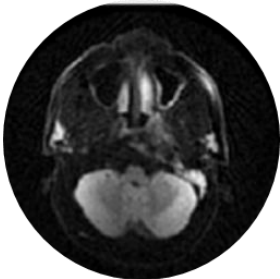
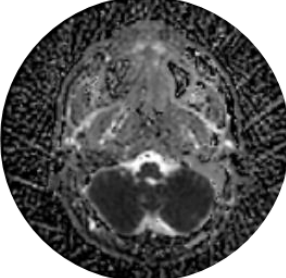
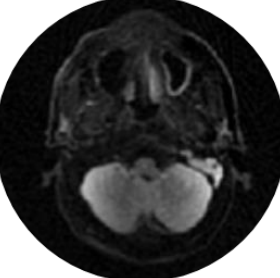
Patient data set		
	Series of ADC image	Series of DWI image
Pre-treatment		
Mid-treatment (5 weeks after CCRT)		

Figure 14 A series of MRI image in patient data set at pre-and mid-treatment

3.7.2 Data analysis

3.7.2.1 Region of interest analysis.

Regions of interest (ROIs) were manually drawn over primary tumor-bearing slice of NPC on DWI image (Fig.15) by information from MRI in others phase at pre-treatment and mid-treatment. All manual ROI of the primary tumor were performed by one experienced neuroradiologist using 3D slicer program and export segmentation data in the NRRD (.nrrd) file format.

A reduction in size for each tumor was calculated base of ROI into percentage change of volume at mid-treatment from pre-treatment given by

$$\% \Delta Vol = 100 \times \frac{(V_P - V_M)}{V_P},$$

where V_P is lesion volume at pre-treatment and V_M is lesion volume at 5 weeks after the initiation of therapy.

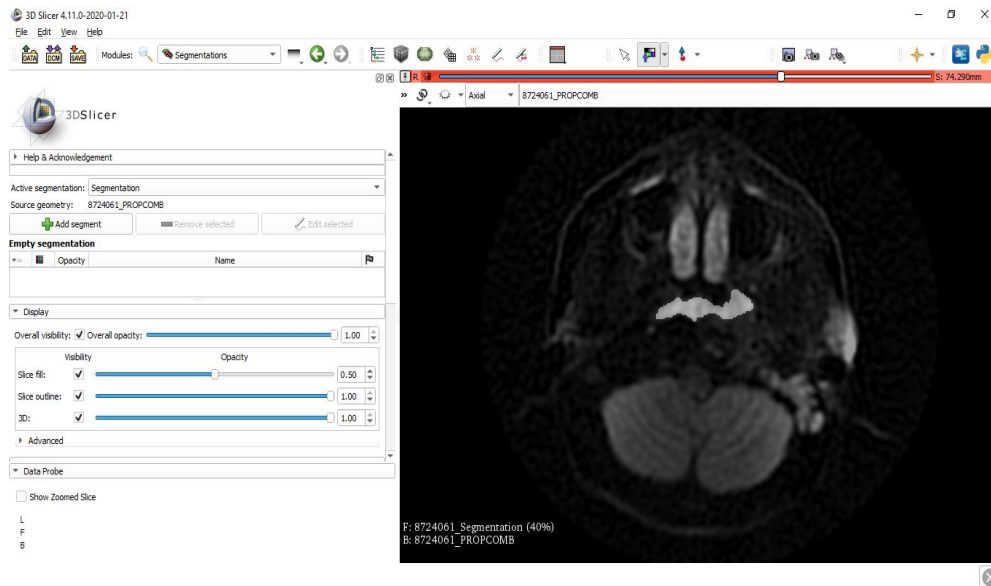


Figure 15 Image of ROI on DWI image in 3D slicer program

3.7.2.2 ADC analysis.

ADC analysis is a method that calculated the mean of water diffuse in the tumor represent in percentage change of whole tumor ADC in lesion at mid-treatment were calculated relative to the pre-treatment value follow by

$$\% \Delta ADC = 100 \times \left(\frac{ADC_M - ADC_P}{ADC_P} \right),$$

where ADC_P and ADC_M represent average ADC value in lesion at pre-treatment, and 5 weeks after the initiation of therapy, respectively.

3.7.2.3 PRM analysis.

To improve ability to define spatial and temporal changes in the tumor during treatment, this study used parametric response mapping (PRM). PRM analysis is based on voxel-wise subtraction, which requires that pre-treatment and mid-treatment images are aligned.

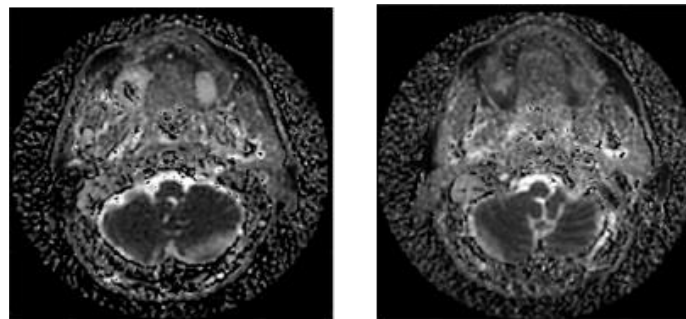
Image registration were performed in serial MR images co-registered from pre-treatment, and follow-up image at five weeks using affine registration of mono-modal image registration using mutual information algorithm in order to optimized the registration process on MATLAB (see Fig.16). Mutual

information algorithm is a quantitative measure of how similar the images are. These algorithms use the joint probability distribution of a pixels from two images to measure the certainty that the values of one set of pixels' map to similar values in the other image.

The researcher performed a two-step registration in order to minimize potential registration errors. First, the DWI image of mid-treatment (moving image) were co-registered to DWI pre-treatment (fixed image) by “imregister” command as follow

$$moving_{reg} = imregister(moving, fixed, transformType, optimizer, metric)$$

where moving is DWI image at mid-treatment, fixed is DWI image at pre-treatment. Both moving and fixed images are the same dimensionality. “transformType” is affine transformation consisting of translation, rotation, scale, and shear. Optimizer is “regularStepGradientDescent”, and metric is mutual information. As the result, the researcher generated the geometrical transformation of registration. Next, used the result of geometric transformation matrix that relates moving to fixed image. Use “imregister” applied to the mid-treatment ADC map.



(a)

(b)

Figure 16 ADC image of mid-treatment in (a) the original image and (b) the registered image.

After registration, The PRM of ADC was calculated the difference between the ADC in mid-treatment and pre-treatment for each voxel ($\Delta ADC = \text{mid-treatment ADC in lesion} - \text{pre-treatment ADC in lesion}$). Each voxel will be classified according its corresponding ΔADC and a threshold that designates a significant change in ADC. In this study, the researcher used the predefined threshold of $100 \times 10^{-5} \text{ mm}^2/\text{sec}$ defined after experimenting with several values.

Specifically, the PRM analysis will classify voxels within tumor into three categories based on ΔADC after mid-treatment. A voxel with ADC increasing of more than a pre-defined threshold will be classified as significantly increased and displayed in red ($\Delta\text{ADC} > 100 \times 10^{-5} \text{ mm}^2/\text{sec}$).

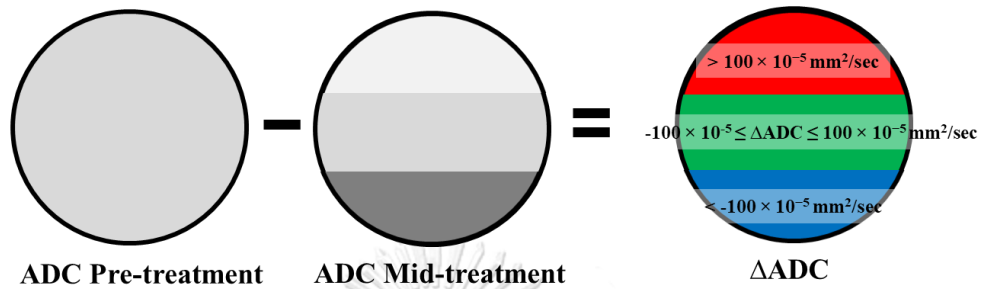


Figure 17 Construction of PRM of ADC are built by using tumor images at pre- and mid-treatment, a difference image is calculated. A significant decrease, increase, and no change in ADC is labelled in blue, red, and green.

A voxel with ADC decreasing by more than the threshold will be classified as significantly decreased and displayed in blue ($\Delta\text{ADC} < -100 \times 10^{-5} \text{ mm}^2/\text{sec}$). Any voxel whose absolute value of ADC change less than the threshold will be classified as no significant change in ADC and will be displayed in green ($-100 \times 10^{-5} \leq \Delta\text{ADC} \leq 100 \times 10^{-5} \text{ mm}^2/\text{sec}$) (Fig.17).

The percentage PRM in each category can be obtained by PRM_+ (increased ADC), PRM_- (decreased ADC), PRM_0 (unchanged ADC) as follow:

$$\text{PRM}_+ = \frac{\text{Number of red voxels}}{\text{Total number of voxels}} \times 100,$$

$$\text{PRM}_- = \frac{\text{Number of blue voxels}}{\text{Total number of voxels}} \times 100,$$

$$\text{PRM}_0 = \frac{\text{Number of green voxels}}{\text{Total number of voxels}} \times 100,$$

where PRM_+ , PRM_0 , PRM_- are the percentage within the tumor of red voxels, green voxels, and blue voxels, respectively. For PRM analysis, this study was focused on only the percentage of voxel with significant increase ADC (PRM_+) for the statistical analysis⁽³³⁾. The distribution changes in PRM of ADC at each time point for the entire tumor volume can illustrate by the scatter plots. The pre-treatment ADC on the x-axis and mid-treatment ADC on the y-axis.

3.7.3 Classification

Each patient will be classified complete-response (CR) or partial-response (PR) using the response evaluation criteria in solid tumors (RECIST) criteria version 1.1⁽³⁷⁾ by a radiologist, which is the clinical standard assessment tool for measuring tumor treatment response. The treatment response will be determined by evaluating axial unidimensional measurements (UDM) on measuring the maximum diameter of the primary tumor and lymph nodes in the largest axial slice of CT and/or MRI at pre-treatment and 6 months after initiation of the treatment.

3.8 Statistical analysis

From the data of DWI in each of the CR and PR groups were obtained the mean and the standard deviation (SD) of $\% \Delta \text{Vol}$, $\% \Delta \text{ADC}$ and PRM_+ . An unpaired two-tailed t-test was used to the determined value of tree biomarkers assessed between a patient with a complete response and partial response.

The test performance for determining whether $\% \Delta \text{Vol}$, $\% \Delta \text{ADC}$ and PRM_+ correlated with tumor control at 6 months were determined using receiver operating characteristic (ROC) curve analysis. ROC curve is a plot of the sensitivity or true-positive rate (y-axis) and 1- specificity or false-positive rate (x-axis) in over all possible cut-points for each biomarker. Moreover, for each biomarker also computed the optimal cutoff point for classify patient group using Youden's J statistic for each biomarker ($\% \Delta \text{Vol}$, $\% \Delta \text{ADC}$ and PRM_+). The Youden's J index, can be formally defined as the maximum vertical distance between the ROC curve and random line (Youden's J = sensitivity + specificity - 1). For a test with poor diagnostic accuracy, Youden's index equals 0, and a perfect test will have a Youden's index of 1⁽³⁸⁾.

The area under the curve (AUC) represents the overall predictive value across all optimal cutoff point, the closer this AUC is to 1 is the stronger ability of the test, whereas an AUC of 0.5 indicates that the test is no better in predicting the condition than tossing a coin.

The test to the evaluation of the performance of the biomarker compare with random guessing was performed using Mann–Whitney U test. Statistical computations were performed using SPSS version 22 (SPSS Inc., Chicago, IL, USA), *p* value of less than 0.05 was considered statistically significant.

3.9 Ethical consideration

The data were collected in the patient data set, initial study was approved by Institutional Review Board (IRB) of the Faculty of Medicine, Chulalongkorn University, Bangkok, Thailand (IRB No. 255/62). The certificate is shown in APPECDIX B.

However, the patient data were collected parallel with the research project entitled “The utility of diffusion-weighted magnetic resonance imaging in predicting treatment response of nasopharyngeal carcinoma” (IRB No. 014/61) but our current work adds the PRM analysis of data and statistical analysis of data.



Chapter IV

RESULTS

4.1 Quality control of MRI system

The quality control of MRI system was performed in the cylindrical Magphan® 170. The performance includes image uniformity, high contrast resolution, low contrast sensitivity, and geometric distortion (spatial linearity). The results are shown in APPENDIX A.

4.2 Patient data

Of the initially enrolled 31 patients with nasopharyngeal carcinoma were initially in the study and 5 patients were subsequently excluded for the following reasons: change of treatment and lost to follow-up at KCMH. A total of 26 patients were used in the analysis to determine the differences in $\% \Delta \text{Vol}$, $\% \Delta \text{ADC}$ and PRM_+ between pre- and mid-treatment (5 female and 21 male patients with mean age of 45 ± 12.4 years). All patients were classified as NPC with locally advanced stage II to IVA following 8th edition TNM Classification of head and neck cancer staging from the American Joint Committee on Cancer (AJCC2018) ⁽³⁹⁾ and each of them had one primary lesion. The clinical characteristics of the patients are listed in Table 3. Patients were stratified by clinical outcome at 6 months which resulted in twenty complete-responders (CR) and six partial-responders (PR).

Table 3 Clinical characteristic of patients

Variable	All patients (N=26)	Complete-response (N=20)	Partial-response (N=6)
Age (year)	45	43	48
Range (year)	18-64	20-63	18-64
Sex (cases)			
Male	21	16	5
Female	5	4	1
Staging (cases)			
II	9	7	2
III	8	7	1
IVA	9	6	3
Mean volume Pre (mm ³)	3,063	3,395	2,532
Mean volume Mid (mm ³)	607	723	492
Mean ADC Pre (10 ⁻⁵ mm ² /sec)	8,268	7,979	8,821
Mean ADC Mid (10 ⁻⁵ mm ² /sec)	12,893	13,059	12,617

Abbreviations: Pre = pre-treatment; Mid = mid-treatment

The representative cases of PRM analysis of CR and PR patients are displays in Fig. 18, 19. Regions of interest were circumscribed on tumor overlaid on unregistered ADC image at pre-treatment as well as the corresponding scatter plots for quantification and distribution of pre-treatment ADC value (y-axis) vs mid-treatment ADC value (x-axis) for the entire tumor volume. Color coding is as follows: red for; voxels with significant increase in ADC; green for; voxels with unchanged ADC; and blue for; voxels with significant decrease in ADC.

Fig. 18 displays images from a patient who was classified as CR, where 92.4% of the tumor volume were found to have a significant increase in ADC (shown as red voxels), regions within the tumor volume, approximately 3.6%, were found to have a significant drop in ADC (shown as blue voxels) and 4.1% unchanged in ADC (shown in green voxel). In comparison, the PR patient (Fig. 19) had only 63.0% of the tumor volume producing a significant increase in ADC and 7.3% of the tumor was found to have a significant decrease in ADC and 29.7% unchanged in ADC (shown in green voxel). Clearly, the results indicated that PRM₊ was higher in a CR patient than in a PR patient.

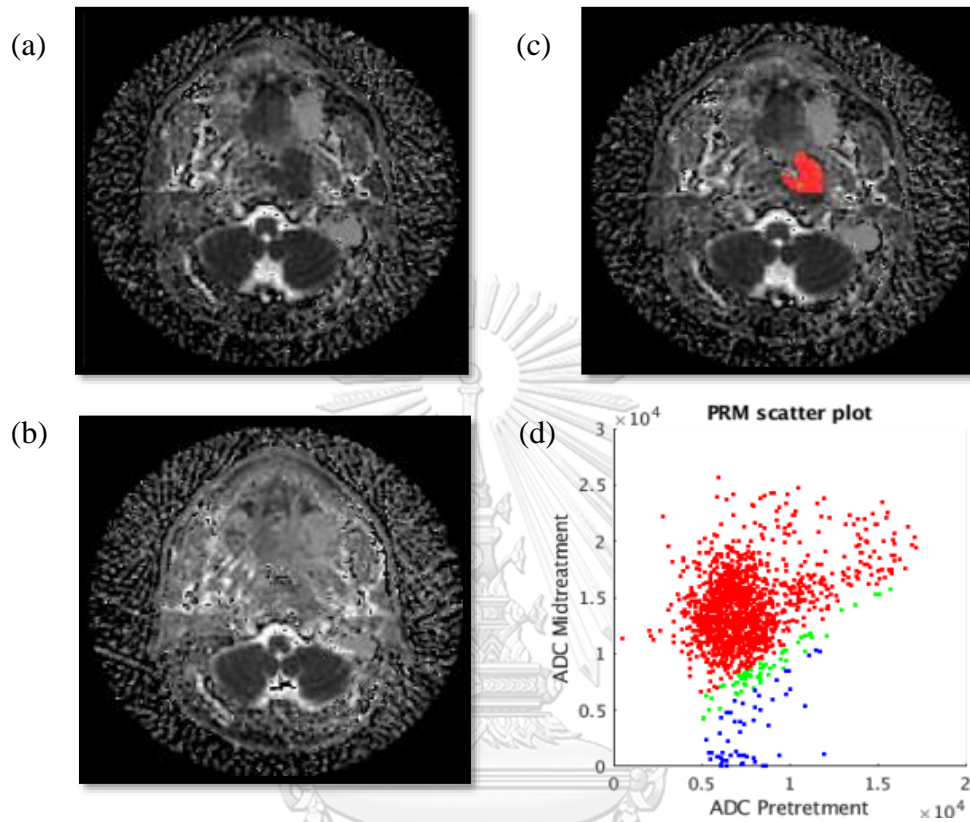


Figure 18 A representative case of CR patients. (a) Axial view of ADC phase at pre-treatment of nasopharynx. (b) mid-treatment ADC image at 5 weeks after CCRT started. (c) PRM overlaid on unregistered ADC image at pre-treatment. (d) The scatter plot illustrates the distribution of changes in PRM throughout the entire volumes of interest. Voxels with significant increase, unchanged, or decrease in ADC values are assigned as red (92.4%), green (4.1%) and blue (3.6%), respectively.

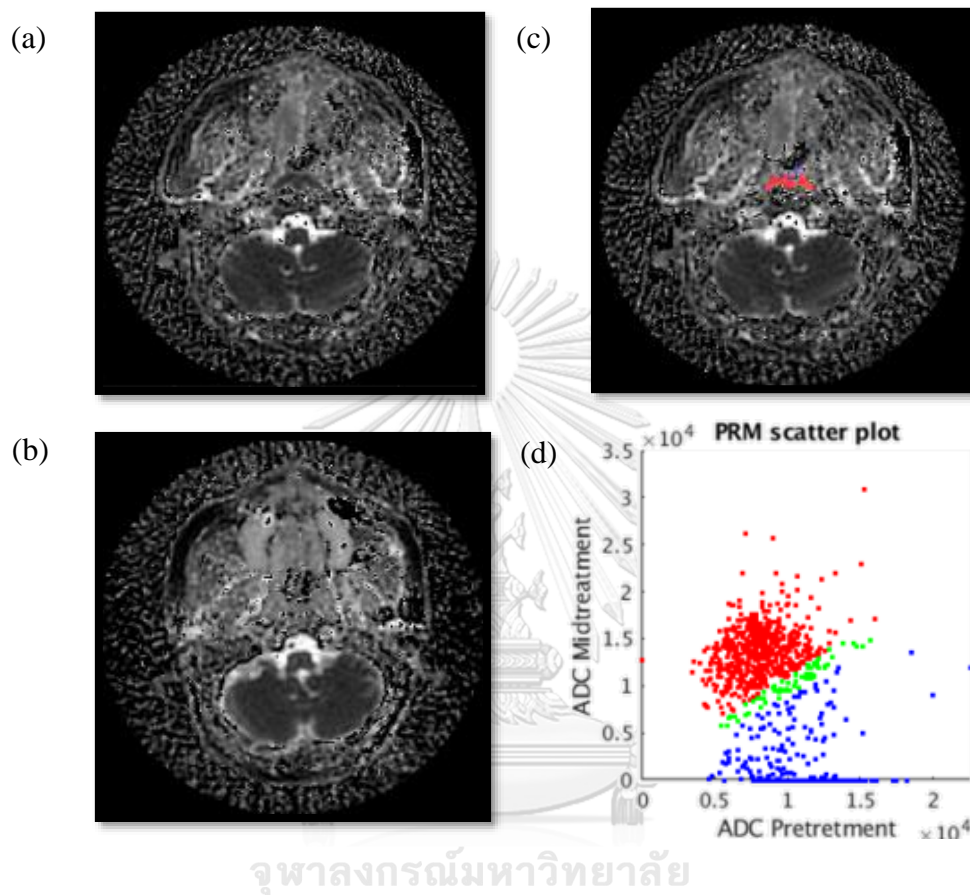


Figure 19 A representative case of PR patients. (a) Axial view of ADC phase at pre-treatment of nasopharynx. (b) mid-treatment ADC image at 5 weeks after CCRT started. (c) PRM overlaid on unregistered ADC image at pre-treatment. (d) The scatter plot illustrates the distribution of changes in PRM throughout the entire volumes of interest. Voxels with significant increase, unchange or decrease in ADC values are assigned as red (63.0%), green (7.3%) and blue (29.7%), respectively.

4.3 Response Prediction

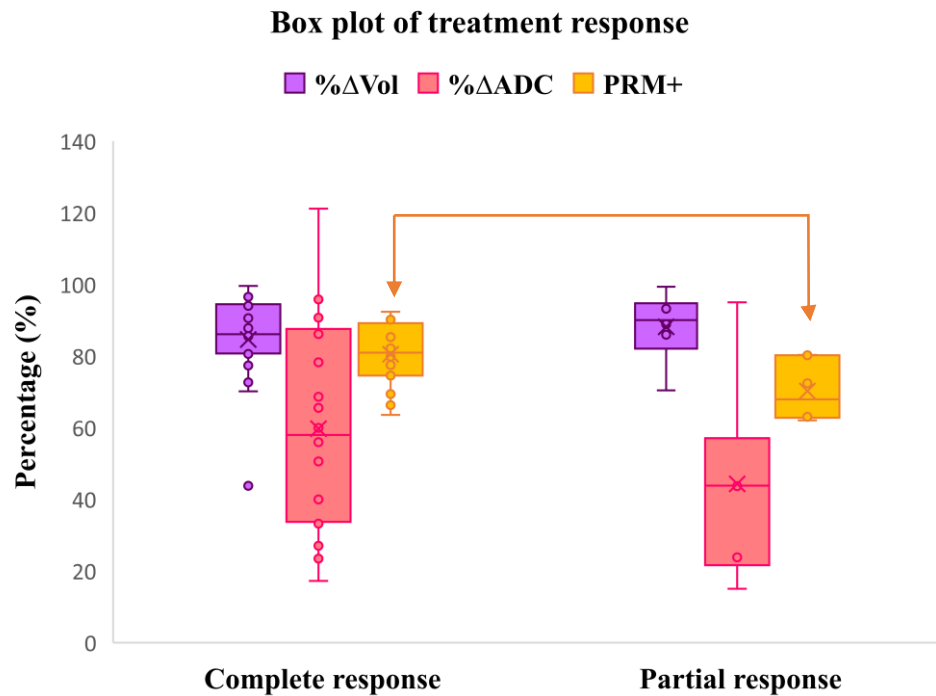


Figure 20 The box plot of three biomarkers: the percentage change of volume (% Δ Vol), the percentage change of ADC (% Δ ADC) and the percentage of voxel with significant increase ADC (PRM₊). The significant difference between both groups of patients was as assessed by t-test with $p < 0.05$.

According to the statistical analysis, % Δ Vol were a large change in tumor volume at pre-treatment and five weeks after initiation of chemoradiationtherapy. The mean value of percentage change (% Δ Vol) in tumor volume did not show a significant difference between CR (mean value = $84.6\% \pm 12.3$) and PR (mean value = $88.2\% \pm 4.5$) with $p = 0.53$. In this study, no patient showed an increase in tumor volume at the end of chemoradiation therapy.

On the other hand, the mean of percentage changes in ADC (% Δ ADC) was higher in mid-treatment as compared with pre-treatment in both patient groups. (mean ADC at pre-treatment = $8268 \text{ mm}^2/\text{sec}$; mean ADC at mid-treatment = $12896 \text{ mm}^2/\text{sec}$). The difference between both patient groups did not show any significant difference ($59.7 \pm 28.4\%$ in CR vs $44.3 \pm 23.7\%$ in PR, $p = 0.26$). The results of treatment response of % Δ Volume, % Δ ADC and PRM₊ are presented in Table 4.

With PRM analysis, it was found that PRM₊ was significantly different between CR and PR groups ($82.7 \pm 7.8\%$ in CR vs $66.7 \pm 6.5\%$ in PR, $p < 0.05$) as shown in Table 4. and Fig 20 (in orange color). Fig 21 displays the treatment response of three

biomarkers of CR and PR patient. In $\% \Delta \text{ADC}$ and $\% \Delta \text{Vol}$ shown negligible differences between clinical groups. PRM_+ of CR patient's medians (lines through boxes) are lower than those of PR patients. Data collection for each patient are shown in Table 5.

Table 4 Treatment response of $\% \Delta \text{Volume}$, $\% \Delta \text{ADC}$ and PRM_+

Biomarker	Patient groups				<i>p</i> -value
	CR		PR		
	Mean	SD	Mean	SD	
$\% \Delta \text{Volume}$	84.63	12.27	88.17	4.51	0.535
$\% \Delta \text{ADC}$	59.70	28.39	44.32	23.75	0.263
PRM_+	80.51	8.55	70.23	7.10	0.018

* Statistically significant at p -value = 0.05.

Table 5 Data collection of each NPC patients

No	Clinical outcome		SEX 0 = F 1 = M	AGE (year)	TNM Staging	1 st DWI (DD/MM/YY)	2 nd DWI	Volume mm ³		ADC mm ² /sec		%ΔVol	%ΔADC	PRM ₊	PRM ₋	PRM ₀
	CR/PR							Pre	Mid	Pre	Mid					
1	CR	0	52	2	18/12/17	12/02/18	1976	78	7558	16714	96.05	121.14	77.47	16.14	6.37	
2	CR	1	53	4A	25/12/17	12/02/18	3008	822	9159	11930	72.67	-28.62	80.98	9.20	9.80	
3	CR	1	38	2	25/12/17	5/02/18	859	91	8014	12067	89.40	50.57	74.62	17.34	8.03	
4	PR	1	56	2	19/02/18	2/04/18	1859	206	7881	11323	88.91	43.67	80.31	15.22	4.46	
5	CR	1	28	3	26/02/18	19/04/18	407	79	8952	14318	80.58	59.94	90.17	2.21	7.61	
6	CR	1	18	4A	26/02/18	18/04/18	3942	137	7041	13428	96.52	90.71	86.17	7.66	6.16	
7	CR	0	46	4A	23/07/19	31/08/18	7066	29	8715	11608	99.58	33.19	74.54	6.61	8.84	
8	CR	1	49	3	21/03/18	28/05/18	1373	410	8168	15993	70.13	95.80	90.75	5.46	3.78	
9	CR	1	50	2	18/01/18	16/02/18	1935	270	7148	12743	86.04	78.27	90.90	4.90	4.18	
10	PR	1	56	4A	26/11/18	14/01/18	1283	180	8686	12502	85.97	43.93	72.40	16.44	11.14	
11	CR	0	26	3	8/11/18	26/12/18	3557	492	7657	14407	86.16	88.01	83.80	9.95	6.24	
12	PR	1	39	4A	30/04/18	31/06/18	903	80	8993	12988	91.14	44.42	63.01	29.67	7.30	
13	CR	1	64	3	10/11/18	13/12/18	2162	398	9461	13241	81.59	39.95	80.94	14.89	4.16	
14	CR	1	47	4A	23/04/18	8/06/18	1547	189	7485	12660	87.78	88.14	92.37	3.55	4.07	

No	Clinical outcome		SEX 0 = F 1 = M	AGE (year)	TNM Staging	1 st DWI (DD/MM/YY)		2 nd DWI		Volume mm ³		ADC mm ² /sec		%ΔVol	%ΔADC	PRM ₊	PRM ₋	PRM ₀
	CR/PR					Pre	Mid	Pre	Mid	Pre	Mid	Pre	Mid					
15	CR		1	33	2	07/11/18	24/12/18	2730	257	7239	11290	90.58	55.96	63.58	26.73	9.67		
16	PR		1	63	2	02/4/18	30/05/18	398	27	9291	11503	93.21	23.80	62.06	20.35	17.58		
17	CR		1	31	3	07/11/18	21/12/18	1404	266	9027	14943	81.05	65.53	79.84	12.17	7.97		
18	PR		0	52	4A	01/11/18	24/12/18	8250	2442	9836	11315	70.40	15.03	80.23	8.10	11.66		
19	CR		1	32	3	28/02/18	18/04/18	1656	99	9143	10717	94.02	17.21	66.30	24.03	9.66		
20	CR		1	53	4A	26/03/18	07/05/18	17555	9867	5355	15197	43.79	-23.46	92.23	4.56	3.19		
21	CR		1	44	2	22/05/18	04/07/18	1404	203	7979	11199	85.54	40.35	69.37	20.01	10.61		
22	CR		1	59	4A	31/05/18	19/07/18	13317	457	8860	11987	96.56	35.29	85.30	8.50	6.19		
23	PR		1	20	3	03/01/19	27/02/19	2499	16	8241	16072	99.35	95.02	63.38	23.20	13.40		
24	CR		0	53	3	20/03/19	13/05/19	574	130	7335	13655	77.35	86.16	69.68	19.51	10.80		
25	CR		1	37	2	26/03/19	29/05/19	902	157	7492	9976	82.59	27.03	82.15	12.30	5.54		
26	CR		1	54	2	01/04/19	27/05/19	520	28	7783	13123	94.61	68.61	79.03	14.23	6.73		

Abbreviations: Pre = pre-treatment; Mid = mid-treatment, CR = complete-response, PR = partial-response

4.4 ROC analysis

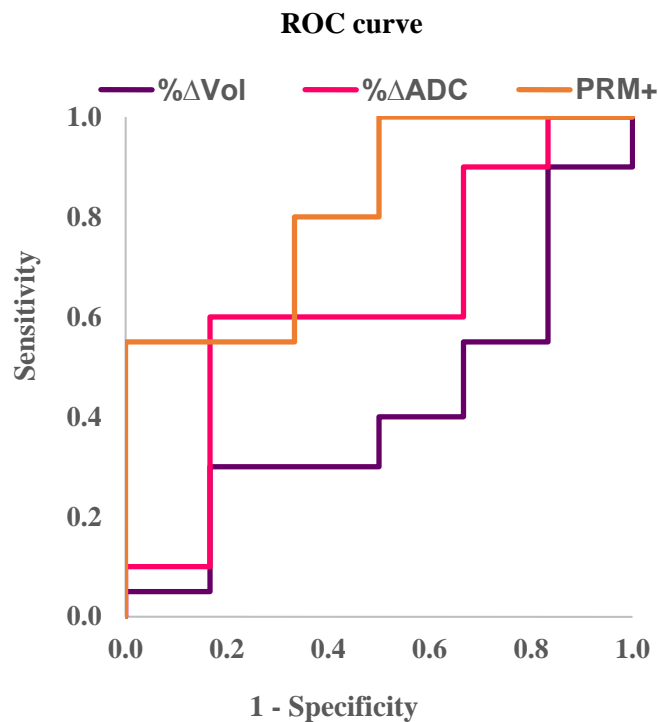


Figure 21 Receiver operating characteristic (ROC) curves of PRM₊ (orange line), %ΔADC (pink line) and %ΔVol (purple line) for predicting treatment response in twenty-six patients with NPC. Area under ROC curves were 0.817, 0.633, and 0.417, respectively.

A receiver operating characteristic (ROC) curve was generated for each of three biomarkers to compare the performance for predicting treatment response. Table 6 presented the AUC value and the optimal cut off point for each of the three biomarkers. As can be seen in Fig.21 and Table 6, PRM₊ showed the highest AUC than %ΔADC and %ΔVol (0.817, 0.633, and 0.417 for PRM₊, %ΔADC and %ΔVol, respectively) and the optimal cut of point using Youden's J statistic of PRM₊, %ΔADC, and %ΔVol to predict CR and PR was 80.62%, 47.49%, and 93.62%. Result of the Youden's J index are presented in Table.7.

In addition, the AUC value of less than 0.5 indicates that the test performs worse than random guessing. Moreover, only PRM₊ was significantly different from random guessing (*p*-value was 0.021), while %ΔADC and %ΔVol were not.

Table 6 ROC curve correlated with treatment outcome

MRI Biomarker	AUC	95% confidence interval	Significant level	Optimal cutoff point
%ΔVol	0.417	0.16 to 0.67	$p = 0.542$	93.62
%ΔADC	0.633	0.33 to 0.37	$p = 0.330$	47.49
PRM₊	0.817	0.09 to 0.63	$p = 0.021$	80.62

Abbreviations: AUC = area under the curve



Table 7 Youden's J index and optimal cut of point of % Δ Volume, % Δ ADC and PRM₊

Variable	The optimal cut of point	Sensitivity	1 - Specificity	Youden's J index
% Δ Vol	42.7938	1.000	1.000	0.00
	56.9661	.950	1.000	-0.05
	70.2692	.900	1.000	-0.10
	71.5365	.900	.833	0.07
	75.0124	.850	.833	0.02
	78.9708	.800	.833	-0.03
	80.8219	.750	.833	-0.08
	81.3226	.700	.833	-0.13
	82.0927	.650	.833	-0.18
	84.0678	.600	.833	-0.23
	85.7559	.550	.833	-0.28
	86.0085	.550	.667	-0.12
	86.1073	.500	.667	-0.17
	86.9755	.450	.667	-0.22
	88.3508	.400	.667	-0.27
	89.1626	.400	.500	-0.10
	89.9962	.350	.500	-0.15
	90.8634	.300	.500	-0.20
	92.1784	.300	.333	-0.03
	93.6189	.300	.167	0.13
94.3186	.250	.167	0.08	
95.3340	.200	.167	0.03	
96.2886	.150	.167	-0.02	
96.5465	.100	.167	-0.07	
97.9640	.050	.167	-0.12	
99.4747	.050	0.000	0.05	
100.5896	0.000	0.000	0.00	
% Δ ADC	14.0366	1.000	1.000	0.00
	16.1244	1.000	.833	0.17
	20.3379	.950	.833	0.12
	23.6358	.900	.833	0.07
	25.4202	.900	.667	0.23
	27.8265	.850	.667	0.18
	30.9082	.800	.667	0.13
	34.2446	.750	.667	0.08
	37.6235	.700	.667	0.03
	40.1547	.650	.667	-0.02
	42.0153	.600	.667	-0.07
	43.8038	.600	.500	0.10
	44.1781	.600	.333	0.27
	47.4987	.600	.167	0.43
	53.2674	.550	.167	0.38
	57.9514	.500	.167	0.33
	62.7393	.450	.167	0.28
	67.0739	.400	.167	0.23
	73.4424	.350	.167	0.18
	82.2179	.300	.167	0.13
87.0896	.250	.167	0.08	
88.0834	.200	.167	0.03	
89.4306	.150	.167	-0.02	
92.8682	.100	.167	-0.07	
95.4128	.100	0.000	0.10	
108.4720	.050	0.000	0.05	
122.1432	0.000	0.000	0.00	
PRM ₊	61.0603	1.000	1.000	0.00
	62.5363	1.000	.833	0.17
	63.1988	1.000	.667	0.33
	63.4876	1.000	.500	0.50
	64.9470	.950	.500	0.45
	67.8388	.900	.500	0.40
	69.5298	.850	.500	0.35
	71.0474	.800	.500	0.30
	73.4743	.800	.333	0.47
	74.5809	.750	.333	0.42
	76.0507	.700	.333	0.37
	78.2591	.650	.333	0.32
	79.4409	.600	.333	0.27
	80.0368	.550	.333	0.22
	80.2712	.550	.167	0.38
	80.6278	.550	0.000	0.55
	80.9638	.500	0.000	0.50
	81.5674	.450	0.000	0.45
	82.9787	.400	0.000	0.40
	84.5556	.350	0.000	0.35
85.7395	.300	0.000	0.30	
88.1733	.250	0.000	0.25	
90.4611	.200	0.000	0.20	
90.8273	.150	0.000	0.15	
91.5701	.100	0.000	0.10	
92.3041	.050	0.000	0.05	
93.3723	0.000	0.000	0.00	

Chapter V

DISCUSSION AND CONCLUSIONS

5.1 Discussion

MRI is a very powerful tool for oncologic imaging, including imaging in nasopharyngeal carcinoma. Several MRI sequence, such as diffusion weighted (DW), dynamic contrast-enhanced (DCE) and functional MRI (fMRI) sequences are capable of characterizing tumor biology and provide functional parameters within tissue.

Nowadays, advanced radiation therapy requires precise MRI images for contouring, characterizing tumor, providing quantitative functional parameters, and monitoring treatment response during and after radiation therapy; hence, the MRI simulation was developed and incorporated into radiation treatment planning process⁽⁴⁰⁾. The MRI simulator has different purpose and technical requirements from diagnosis MRI. It requires a large scanning bore with more than 70 cm for immobilization setup, a flat couch top, and an external laser positioning system in the MRI room⁽⁴¹⁾.

In our study, imaging data were acquired on MRI simulation for radiation treatment planning before treatment verification at pre-treatment and MRI at mid-treatment with thermoplastic immobilization masks. The immobilization mask was made fit with an individual patient to prevent the patient's head and neck from moving. According to the treatment course, the anatomy of a patient who gets the chemoradiation will change during treatment; therefore, images acquired from two time points will be mismatched, and cannot be readily used for PRM analysis. To align the images from two time points, we need to perform image registration.

Currently, the intratumor heterogeneity has been reported to have pronounced effects on diagnosis and prognosis of NPC, and thus it is considered to be a potential predictive factor of NPC⁽⁴²⁾. PRM analysis derived from MRI has been reported to be an effective biomarker for early cancer treatment response prediction by looking at change of tissue function within tumor, which reflects intratumoral heterogeneity.

Our results indicated that PRM analysis on ADC from DWI had the potential for early treatment response prediction in NPC patients at five weeks after treatment. Comparing between $\% \Delta \text{ADC}$ and $\% \Delta \text{Vol}$, the AUC for predicting response when using PRM₊ as biomarker was higher than using $\% \Delta \text{ADC}$, and $\% \Delta \text{Vol}$.

Early prediction of response to treatment is essential to avoid inefficient treatment of individual patients and improve the entire health care system. Our study utilized ADC at pre- and 5 weeks after initiation of the CCRT validates PRM₊ as biomarker because it followed the routine protocol at KCMH that patients have to follow-up at 5 weeks after the treatment starts.

In 2009, Galbán, *et al.* ⁽³²⁾ investigated the feasibility of using PRM analysis for DW-MRI data as an early biomarker for monitoring therapeutic efficacy following chemoradiationtherapy (CRT) in patients with head and neck cancer. The result indicated that the percentage change of ADC in 3 weeks after therapy have no significant difference. Nevertheless, this was different from our results that $\% \Delta \text{ADC}$, and $\% \Delta \text{Vol}$ showed no difference between CR and PR groups (see Table.8).

These can be explained as follows. Their work focused on head and neck (H&N) cancer including the nasopharynx, oropharynx, and hypopharynx where most of them were non-NPC, which was different from our work that focused only on nasopharyngeal carcinoma. Although NPC is one of H&N cancers, its characteristics are different from other H&N cancers in its occurrence, causes, clinical behavior, and treatment. Another possible reason is the definition of ROI. In their work, ROI included both primary tumor and lymph nodes, while we defined ROI as only primary tumor in our work.

In our work, that $\% \text{Vol}$ and $\% \text{ADC}$ did not perform well in predicting CR or PR may be because RECIST criteria used to define CR and PR involves several parameters such a target size or lymph node. Therefore, the biomarker from PRM analysis was significantly different between CR and PR groups which was consistent with our results. It could be explained that PRM was more predictive for CR and PR because PRM indicated heterogeneity, where Vol and ADC did not. This may be because the effect of treatment is pronounced in tissue functional processes earlier than in anatomical structures. Moreover, PRM₊ had higher AUC than $\% \Delta \text{ADC}$, which was resulted from the fact that PRM₊ is a voxel-based technique accounting for heterogeneity in the tumor and is more sensitive than a whole-tumor technique, such as $\% \Delta \text{ADC}$.

However, our study had limitations. First, our study was a preliminary result which was based on small sample size. Second, NPC is the cancer that has complex pattern. It may cause possible mismatch between pre-treatment and mid-treatment may occur due to poor registration. Finally, our study used only one MRI follow-up (at five weeks) for NPC patients.

In addition, although this study focused only on NPC patients treated with CCRT, the PRM can, in principle, be applied to most other cancers and treatments given allow diffusion measurements in other body regions and a several time point MRI follow-up may be needed.

Table 8 The comparison of biomarker results between the literature review and this study.

Study	Cancer Type	DW scanning protocol	Treatment	Registration	ROI analyzed	Treatment response	%ΔVolume	%ΔADC	PRM ₊
J. Galbán, et al Translational Oncology (2009) n = 15	Head and neck cancer (oropharynx=12, Nasopharynx=1, Hypopharynx=1, Unknown=1)	3 T; TR/TE: 2789 ms. /59 ms. (b = 0, 1000 s/ mm ²)	Chemoradiation	Deformable registration	Primary tumor and/or Lymph node	CR (n =12)	43 ± 6	Negligible differences	55 ± 4
						PR (n =3)	22 ± 4		37 ± 7
						p value	< 0.05 significant difference	no significant difference	< 0.05 significant difference
Our result n = 26	Nasopharyngeal cancer	1.5 T; TR/TE: 5000 ms. /79.8 ms. (b = 0, 800 s/mm ²)	Chemoradiation (CCRT)	Affine registration	Primary tumor	AUC	0.758	0.758	0.825
						CR (n =20)	84 ± 12	60 ± 28	81 ± 8
						PR (n =6)	88 ± 5	44 ± 24	70 ± 7
						p value	0.535 no significant difference	0.263 no significant difference	< 0.05 (0.02) significant difference
						AUC	0.417	0.663	0.817

5.2 Conclusion

The Heterogeneity in malignancies has been reported to be a potential predictive factor of NPC patients. The observations in this study indicated that the proposed PRM biomarker to quantify the ratio of voxels with significantly increased ADC values as assessed by PRM₊, was significant different in CR and PR with p value < 0.05 . The performance of predicting treatment outcome of CCRT at 6 months in PRM₊ had higher than $\% \Delta \text{ADC}$, and $\% \Delta \text{Vol}$.

The propose of PRM₊ was based on voxel-based analysis which accounted for intratumoral heterogeneity, may be a potential biomarker for early chemoradiation treatment response prediction in NPC. Early prediction of response to treatment is essential in order to improve treatments and related toxicity.



APPENDIX A

Quality control of MRI system

Location:	MRI simulator room, Radiation oncology department, Vongvanich building, King Chulalongkorn Memorial Hospital.
Manufacturer:	GE Medical systems
Model name:	Signa HDxt 1.5 T, Serial number 17085
QC phantom:	Cylindrical Magphan phantom, Model SMR170 (Fig.22)

Quality control of MRI scanners was performed according to Magphan manual in the phantom laboratory as follows:

- Phantom positional verification
- Image uniformity
- High contrast resolution
- Low contrast sensitivity
- Geometric distortion (spatial linearity)

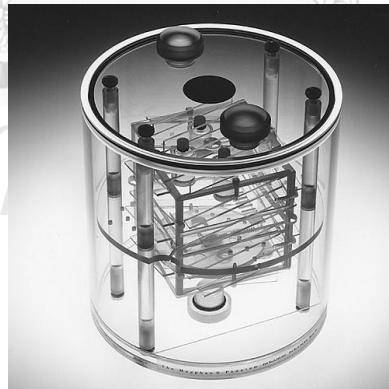


Figure 22 Magphan® SMR 170 phantom

Phantom position verification

Objective: To verify positioning of phantom set-up and alignment for scanning.

Method:

We placed the phantom in the MRI machine with 6 channels flex PA coil. The center of the phantom was placed in the center of coil and aligned with the positioning indicator light along three axes using the plastic level, and the scanner alignment lights as a guide.

Result:

In the localizer image, we could see the slice width ramps protruding from the test cube, and centered the ramp protrusions are opposite each other (see Fig 23).

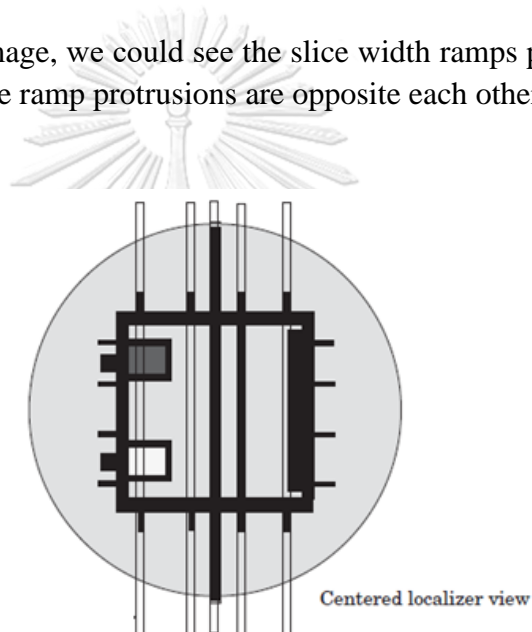


Figure 23 The localizer image of the phantom Magphan with slice locations for axial scans indicated.

Image uniformity

Objective: To test the ability of the MR imaging system to produce a constant signal response throughout the scanned volume when the object is being imaged with homogeneous MR characteristics.

Method:

We displayed the Magphan housing without the test cube and support disk. For image analysis, we placed a large circular ROI at the center of the image of the signal producing volume, enclosing at least 80% of the image, excluding regions near the edge. We determined the maximum (S_{max}) and minimum (S_{min}) pixel values within the ROI by calculating the percent integral uniformity (PIU) as follows:

$$PIU = \left[1 - \frac{(S_{max} - S_{min})}{(S_{max} + S_{min})} \right] \times 100$$

where S_{max} is the maximum pixel value within the ROI, S_{min} is the minimum pixel value within the ROI.



Figure 24 The Magphan® housing without the test cube

Result:

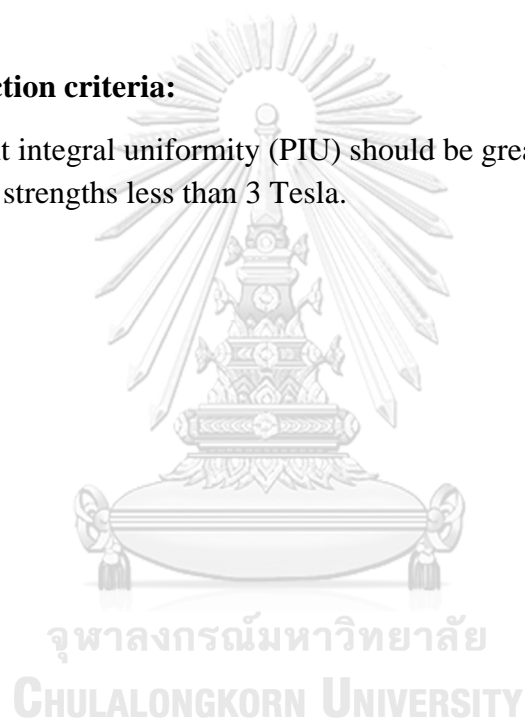
Table 9 The percent integral uniformity (PIU) of the T1 and T2 FS image.

Sequence	No	S_{min}	S_{max}	PIU (%)	Acceptance decision
T1	1	2456	2942	90.96	pass
	2	2416	2931	90.37	pass
	3	2430	2940	90.50	pass

	Average	2434	2938	90.62	pass
Sequence	No	S_{min}	S_{max}	PIU (%)	Acceptance decision
T2 FS	1	3781	4459	91.77	pass
	2	3812	4459	92.17	pass
	3	3781	4440	91.98	pass
	Average	3791	4452	91.98	pass

Recommended action criteria:

The percent integral uniformity (PIU) should be greater than 80 % for MRI systems with field strengths less than 3 Tesla.



High contrast resolution

Objective: To measure the capacity of an imaging system to show separation of objects when there is no significant noise contribution.

Method:

We displayed the high contrast resolution slice and magnify the image. We looked at the smallest resolvable array element and made a note of the smallest target size resolved. The targets were 1, 2, 3, 4, 5, 6, 7, 8, 9, 10, and 11-line pair/cm as in Fig. 25.

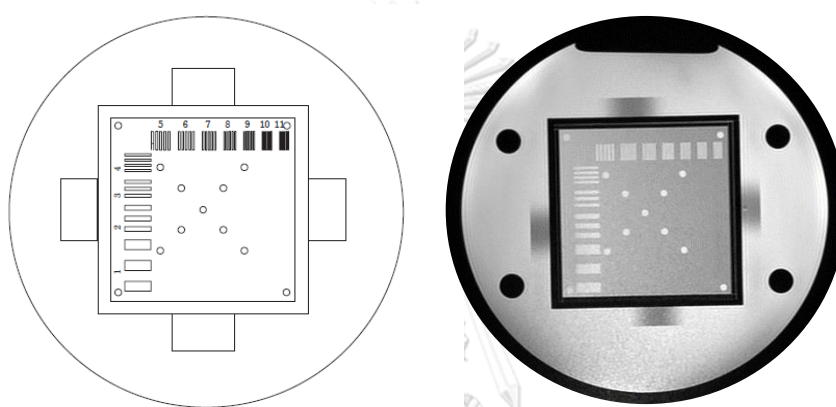


Figure 25 High resolution pattern

Results:

Table 10 The results of high contrast resolution in line pair/cm.

Sequence	Smallest resolvable array element (lp/cm)	Accepted
T1	5 line pair/cm	pass
T2 FS	4-line pair/cm	pass

Recommended action criteria:

The high-contrast resolution should be equal to the pixel size or better (resolution of 1.0 mm or better).

Low contrast sensitivity

Objective: To measure the ability to distinguish differences in intensity in the image.

Method:

We displayed the slice to be scored and adjusted the display window width and level setting for best visibility of low-contrast objects. We determined the actual contrast levels of phantom by making ROI measurements at least 4 x 4 pixels in diameter of the hole, and calculated the average of the measurements from several scans of low contrast section. The Table 11. refer to Fig. 26., the low contrast targets had the following diameters and contrasts:

Table 11 The target diameters and hole depths of the phantom

Target diameters	Hole depths
4.0 mm	0.5mm
6.0 mm	0.75 mm
10.0 mm	1.0 mm
	2.0 mm

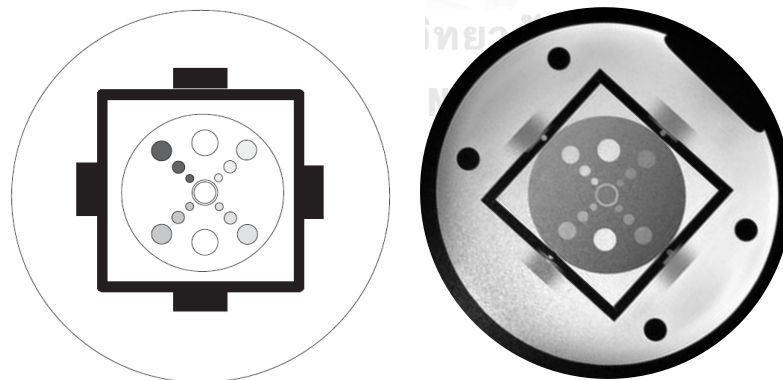


Figure 26 Low contrast pattern

Results:**Table 12** Mean value of pixel intensity for low contrast sensitivity in T1 and T2FS sequence

Sequence	Depths (mm)	Mean value of pixel intensity		
		Diameters (mm)		
		4.0	6.0	10.0
T1	0.5	1710.19	1672.16	1591.68
	0.75	1769.43	1725.37	1607.61
	1.0	2018.25	2019.13	2017.21
	2.0	2426.92	2474.64	2449.88
T2 FS	0.5	2621.15	2599.17	2519.04
	0.75	2820.75	2675.31	2469.64
	1.0	3260.27	3268.08	3302.54
	2.0	3995.73	3959.34	3909.05

Scan Slice geometry (slice width)

Objective: To estimate the full width at half maximum (FWHM) of the slice profile.

Method:

We displayed the slice to be scored of the 4 test planes in the test cube there are two pairs of opposed 14° ramps: one pair is oriented to the x axis, the other pair to the y axis. The ramps are made of 2 mm thick acrylic strips 10 mm wide mounted at 14° angles to the imaging plane. These ramps are used to estimate slice width. The slice width or z(mm) can calculating as follows:

$$Z(mm) = (FWHM)X \times 0.25$$

$$Z(mm) = (FWHM)Y \times 0.25$$

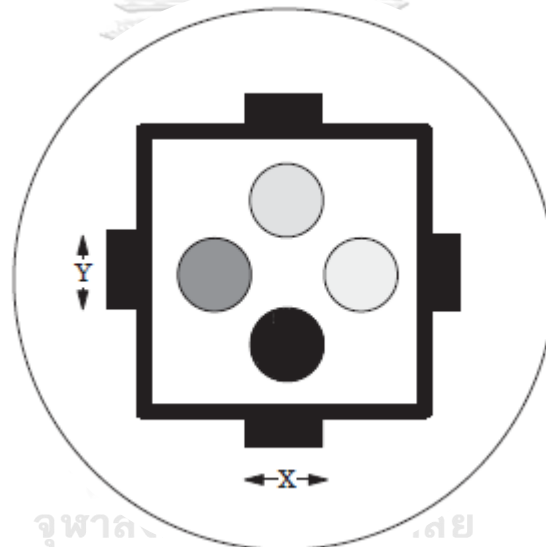


Figure 27 Scan Slice geometry pattern with location of X and Y ramp

To find the FWHM of the ramp from the scan image we need to determine the values for the peak of the ramp, and for the background. To calculate the value for the peak of the ramp, close down your window width. Move the MRI scanner window level to the point where the ramp disappears. Note the number of the level at this occurrence as your peak.

To calculate the value for the background, use the region of interest indicator to identify the mean value of the area adjacent to the ramp. Using the above values determine the Half Maximum by calculate the net peak (net peak = peak value – background value) after that calculate the 50% net peak and calculate half maximum (half maximum = (net peak/2) + background value). To find FWHM we set the MRI scanner window level at the half maximum value and measure the length of the ramp in the image.

Results:**Table 13** The result of slice geometry

Sequence	Ramp	Mean Bg	Half maximum	FWHM (mm)	Z (mm)	Slice thickness (mm)	% Difference
T1	X	2219	1684	16.33	4.0825	4	2%
	Y	2187	1668	16.47	4.1175	4	3%
T2 FS	X	3586	2523.5	15.419	3.85475	4	4%
	Y	3500	2480.5	14.611	3.65275	4	9%

Abbreviations: Bg – Background, FWHM - The full width at half maximum



Geometric distortion

Objective: To assess the accuracy of the image lengths in the imaged subject.

Method:

We measured the displacement of displayed points within an image relative to their known location of the phantom in 4 directions: X, Y, Left and Right (Fig 27,28). The percent distortion was defined as following:

$$\%Distortion = \left(\frac{\text{True dimension} - \text{observed dimension}}{\text{True dimension}} \right) \times 100$$

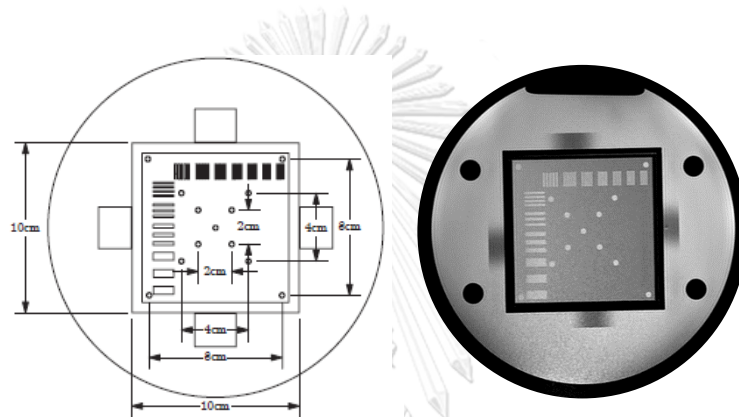


Figure 28 Geometric distortion (spatial linearity) pattern distance X and Y.

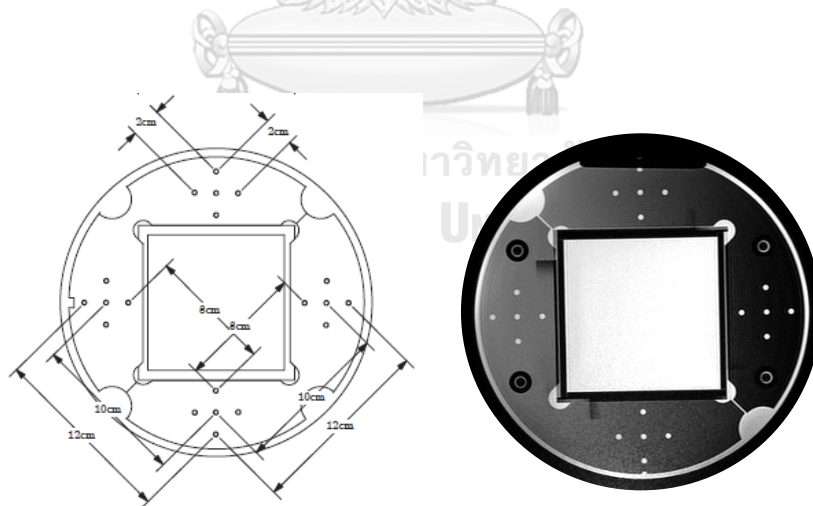


Figure 29 Geometric distortion (spatial linearity) pattern distance left and right.

Results:**Table 14** The results of geometric distortion in X and Y direction.

Sequence	Distance	2 cm	4 cm	8 cm	10 cm
T1	Measured distance (X)	2.04	4.01	8.03	9.99
	% Difference	2%	0.2%	0.4%	0.1%
	Measured distance (Y)	1.97	3.97	8.03	10.01
	% Difference	1.5%	0.7%	0.4%	0.1%
T2 FS	Measured distance (X)	2.02	4.01	8.04	10.01
	% Difference	1%	0.2%	0.5%	0.1%
	Measured distance (Y)	1.99	3.98	8.01	10.04
	% Difference	0.1%	0.5%	0.1%	0.4%

Table 15 The results of geometric distortion in Z direction.

Sequence	Distance	2 cm	8 cm	10 cm	12 cm
T1	Measured distance (R)	2.03	7.99	10.08	12.04
	% Difference	1.5%	0.1%	0.8%	0.4%
	Measured distance (L)	2.02	8.04	10.05	12.05
	% Difference	1%	0.5%	0.5%	0.4%
T2 FS	Measured distance (R)	1.99	7.99	10.01	12.00
	% Difference	0.1%	0.1%	0.1%	0%
	Measured distance (L)	2.02	8.03	10.05	12.05
	% Difference	1%	0.4%	0.5%	0.4%

Table 16 The result of percentage distortion

Sequence	Distortion (%)	Acceptance decision
T1	<5	pass
T2 FS	<5	pass

Recommended action criteria:

Percent distortions in the spatial linearity are generally considered acceptable if they are less than 5%.



Table 17 Overview of parameters for QC testing

Study	Pulse Sequence	MR acquisition type	Number of average	TR (ms)	TE (ms)	FA (flip angle)	ETL (Echo train length)	FOV (cm)	Slice Thickness (mm)	Slice Gap (mm)	Matrix	Band width (Hz)
Axial T1	Spin echo	2D	1	560	8.64	90	4	22	4	4.4	320 x 224	122.07
Axial T2 FS	Spin echo	2D	1	3680	80.90	90	17	22	4	4.4	320 x 256	97.66

Abbreviations: FOV-Field of view, TR-Repetition time, TE-Echo time, FA-Flip angle, Hz-Hertz

APPENDIX B

The approval of institutional review board

Certificate of research approval from Institutional Review Board (IRB) of faculty of Medicine, Chulalongkorn University, Bangkok, Thailand. IRB no. 255/62.



COA No. 613/2019

IRB No. 255/62

INSTITUTIONAL REVIEW BOARD

Faculty of Medicine, Chulalongkorn University

1873 Rama 4 Road, Patumwan, Bangkok 10330, Thailand, Tel 662-256-4493

Certificate of Approval

The Institutional Review Board of the Faculty of Medicine, Chulalongkorn University, Bangkok, Thailand, has approved the following study which is to be carried out in compliance with the International guidelines for human research protection as Declaration of Helsinki, The Belmont Report, CIOMS Guideline and International Conference on Harmonization in Good Clinical Practice (ICH-GCP)

Study Title : A Feasibility Study of Diffusion Weighted Imaging and Parametric Response Map Analysis for Treatment Response Prediction in Nasopharyngeal Cancer.

Study Code : -

Principal Investigator : Miss Titiya Jirawatwanith

Affiliation of PI : Department of Radiology,
Faculty of Medicine, Chulalongkorn University.

Review Method : Expedited

Continuing Report : At least once annually or submit the final report if finished.

Document Reviewed :

1. Research Proposal Version 2 Date 28/05/2019
2. Protocol Synopsis Version 2 Date 28/05/2019
3. Case record form Version 1 Date 22/03/2019
4. Curriculum Vitae and GCP Training
 - Miss Titiya Jirawatwanith

Approval granted is subject to the following conditions: (see back of this Certificate)



- Asst.Prof. Yothin Rakvongthai, Ph.D.

Signature
(Emeritus Professor Tada Sueblinwong MD)
Chairperson
The Institutional Review Board

Signature
(Assistant Professor Thananya Thongtan, PhD.)
Member and Assistant Secretary, Acting Secretary
The Institutional Review Board

Date of Approval : May 31, 2019
Approval Expire Date : May 30, 2020

Approval granted is subject to the following conditions: (see back of this Certificate)

APPENDIX C

Case record form

Table 18 A format of case record form for collect the patient data.

Patient No. □□□	
HN □□□□□□□□□□	
Acquisition date (DD/MM/YYYY) □□ / □□ / □□□□	
Age (year)	
Sex	<input type="checkbox"/> Male <input type="checkbox"/> Female
Smoking	<input type="checkbox"/> Yes <input type="checkbox"/> No
EBV viral load	<input type="checkbox"/> Less than 316 copies/mL (____)
	<input type="checkbox"/> More than 316 copies/mL (____)
Staging	_____, T____ N____ M____
Cell type	<input type="checkbox"/> Well differentiation
	<input type="checkbox"/> Mod differentiation
	<input type="checkbox"/> Poorly differentiation
	<input type="checkbox"/> Undifferentiation
RT +dose (IMRT technique)	
CMT + dose	
ROI by neuroradiologist	
Pre-treatment	Date:
	Mean ADC = _____
	Volume = _____
	Voxel size = _____
	Number of slide = _____

Mid-treatment (5 week)	Date: _____
	Mean ADC = _____
	Volume = _____
	Voxel size = _____
	Number of slide = _____
% ΔVolume	_____
% ΔADC	_____
PRM₊	_____
PRM_.	_____
PRM₀	_____
Response to treatment at 6 months after beginning CCRT	
Imaging	<input type="checkbox"/> MRI <input type="checkbox"/> CT
Clinical outcome	<input type="checkbox"/> Complete- responders <input type="checkbox"/> Partial responders

Table 19 A format of data collection

No	Clinical outcome	SEX	AGE (year)	TNM Staging	1 st DWI (DD/MM/YY)	2 nd DWI	Volume mm ³		ADC mm ² /sec		% Δ Vol	% Δ ADC	PRM ₊	PRM.	PRM ₀	
	CR/PR	0 = F 1 = M			(DD/MM/YY)		Pre	Mid	Pre	Mid			Affine Registration			

Abbreviations: Pre = Pre-treatment, Mid = Mid-treatment

Table 20 A format of test result variable

Test Result Variable	No of patient	The optimal cutoff point	Sensitivity	1 - Specificity	Youden's J index
	1				
	2				
	3				
	4				
	5				
	6				
	7				
	8				
	9				
	10				
	11				
	12				
	13				
	14				
	15				
	16				
	17				
	18				
	19				
	20				
	21				
	22				
	23				
	24				
	25				
	26				

REFERENCES

1. Torre LA, Bray F, Siegel RL, Ferlay J, Lortet-Tieulent J, Jemal A. Global cancer statistics, 2012. *CA Cancer J Clin* 2015;65:87-108.
2. Liu Z, Xu C, Jiang R, Liu G, Liu Q, Zhou J, et al. Treatment of Locally Advanced Nasopharyngeal Carcinoma by Helical Tomotherapy: An Observational, Prospective Analysis. 2019;12:757-63.
3. Glover GHJNC. Overview of functional magnetic resonance imaging. 2011;22:133-9.
4. Obata T, Kershaw J, Tachibana Y, Miyauchi T, Abe Y, Shibata S, et al. Comparison of diffusion-weighted MRI and anti-Stokes Raman scattering (CARS) measurements of the inter-compartmental exchange-time of water in expression-controlled aquaporin-4 cells. 2018;8:1-11.
5. Schwartz K, Lane J, Bolster B, Neff BJAJoN. The utility of diffusion-weighted imaging for cholesteatoma evaluation. 2011;32:430-6.
6. Dietrich TJ, Ulbrich EJ, Zanetti M, Fucentese SF, Pfirrmann CWJAJor. PROPELLER technique to improve image quality of MRI of the shoulder. 2011;197:W1093-W100.
7. Sprawls P. Magnetic resonance imaging: principles, methods, and techniques: Medical Physics Publishing; 2000.
8. Stejskal EO, Tanner JEJtjocp. Spin diffusion measurements: spin echoes in the presence of a time-dependent field gradient. 1965;42:288-92.
9. Ravi S, Khan A. SEGMENTATION OF STROKE REGIONS FROM DWI AND ADC SEQUENCES USING A MODIFIED WATERSHED METHOD.
10. Hulka SJBmie. Overview of biological marker. 1990:3-15.
11. Manne U, Srivastava R-G, Srivastava SJDdt. Keynote review: Recent advances in biomarkers for cancer diagnosis and treatment. 2005;10:965-76.
12. Mercado CLJRC. BI-RADS Update. 2014;52:481-7.
13. Dregely I, Prezzi D, Kelly-Morland C, Roccia E, Neji R, Goh V. Imaging biomarkers in oncology: Basics and application to MRI. *J Magn Reson Imaging* 2018;48:13-26.
14. Hamstra DA, Rehemtulla A, Ross BD. Diffusion magnetic resonance imaging: a biomarker for treatment response in oncology. *J Clin Oncol* 2007;25:4104-9.
15. Baer AH, Hoff BA, Srinivasan A, Galbán CJ, Mukherji SK. Feasibility Analysis of the Parametric Response Map as an Early Predictor of Treatment Efficacy in Head and Neck Cancer. *American Journal of Neuroradiology* 2015;36:757-62.
16. Drisis S, El Adoui M, Flamen P, Benjelloun M, Dewind R, Paesmans M, et al. Early prediction of neoadjuvant treatment outcome in locally advanced breast cancer using parametric response mapping and radial heterogeneity from breast MRI. 2019.
17. Dougherty G. Digital image processing for medical applications: Cambridge University Press; 2009.
18. Abdallah YMY, Alqahtani T. Research in Medical Imaging Using Image Processing Techniques. *Medical Imaging-Principles and Applications: IntechOpen*; 2019.
19. Birkfellner W. Applied medical image processing: a basic course: CRC Press; 2016.

20. Som PM, Curtin HD. Head and Neck Imaging E-Book: Elsevier Health Sciences; 2011.
21. Meyer J, editor Histogram transformation for inter-modality image registration. 2007 IEEE 7th International Symposium on BioInformatics and BioEngineering; 2007: IEEE.
22. Casciato DA, Territo MC. Manual of clinical oncology: Lippincott Williams & Wilkins; 2009.
23. Comoretto M, Balestreri L, Borsatti E, Cimitan M, Franchin G, Lise MJR. Detection and restaging of residual and/or recurrent nasopharyngeal carcinoma after chemotherapy and radiation therapy: comparison of MR imaging and FDG PET/CT. 2008;249:203-11.
24. Amin MB, Greene FL, Edge SB, Compton CC, Gershenwald JE, Brookland RK, et al. The eighth edition AJCC cancer staging manual: continuing to build a bridge from a population-based to a more “personalized” approach to cancer staging. 2017;67:93-9.
25. Blanchard P, Lee A, Marguet S, Leclercq J, Ng WT, Ma J, et al. Chemotherapy and radiotherapy in nasopharyngeal carcinoma: an update of the MAC-NPC meta-analysis. 2015;16:645-55.
26. Cui Y ZX, Sun YS, Tang L, Shen L. Apparent diffusion coefficient: potential imaging biomarker for prediction and early detection of response to chemotherapy in hepatic metastases. Radiology. 2008;248:894–900. Apparent diffusion coefficient: potential imaging biomarker for prediction and early detection of response to chemotherapy in hepatic metastases. . 2008.
27. Harry VN, Semple SI, Gilbert FJ, Parkin DE. Diffusion-weighted magnetic resonance imaging in the early detection of response to chemoradiation in cervical cancer. Gynecol Oncol 2008;111:213-20.
28. Ceschin R, Kurland BF, Abberbock SR, Ellingson BM, Okada H, Jakacki RI, et al. Parametric Response Mapping of Apparent Diffusion Coefficient as an Imaging Biomarker to Distinguish Pseudoprogression from True Tumor Progression in Peptide-Based Vaccine Therapy for Pediatric Diffuse Intrinsic Pontine Glioma. AJNR Am J Neuroradiol 2015;36:2170-6.
29. Ellingson BM, Malkin MG, Rand SD, LaViolette PS, Connelly JM, Mueller WM, et al. Volumetric analysis of functional diffusion maps is a predictive imaging biomarker for cytotoxic and anti-angiogenic treatments in malignant gliomas. J Neurooncol 2011;102:95-103.
30. Reischauer C, Froehlich JM, Pless M, Binkert CA, Koh DM, Gutzeit A. Early treatment response in non-small cell lung cancer patients using diffusion-weighted imaging and functional diffusion maps--a feasibility study. PLoS One 2014;9:e108052.
31. Yabuuchi H, Hatakenaka M, Takayama K, Matsuo Y, Sunami S, Kamitani T, et al. Non-small cell lung cancer: detection of early response to chemotherapy by using contrast-enhanced dynamic and diffusion-weighted MR imaging. Radiology 2011;261:598-604.
32. Galbán CJ, Mukherji SK, Chenevert TL, Meyer CR, Hamstra DA, Bland PH, et al. A Feasibility Study of Parametric Response Map Analysis of Diffusion-Weighted Magnetic Resonance Imaging Scans of Head and Neck Cancer Patients for Providing Early Detection of Therapeutic Efficacy. Translational Oncology 2009;2:184-90.
33. Hamstra DA, Galban CJ, Meyer CR, Johnson TD, Sundgren PC, Tsien C, et al. Functional diffusion map as an early imaging biomarker for high-grade glioma:

- correlation with conventional radiologic response and overall survival. *J Clin Oncol* 2008;26:3387-94.
34. Cohen JH, New Jersey. *Statistical Power Analysis for the Behavioral Sciences—Second Edition*. 12 Lawrence Erlbaum Associates Inc. 1988;13.
 35. Fedorov A, Beichel R, Kalpathy-Cramer J, Finet J, Fillion-Robin J-C, Pujol S, et al. 3D Slicer as an image computing platform for the Quantitative Imaging Network. 2012;30:1323-41.
 36. Schneider CA, Rasband WS, Eliceiri KWJNm. NIH Image to ImageJ: 25 years of image analysis. 2012;9:671-5.
 37. Eisenhauer EA, Therasse P, Bogaerts J, Schwartz LH, Sargent D, Ford R, et al. New response evaluation criteria in solid tumours: revised RECIST guideline (version 1.1). *Eur J Cancer* 2009;45:228-47.
 38. Perkins NJ, Schisterman EFJBJJoMMiB. The Youden Index and the optimal cut-point corrected for measurement error. 2005;47:428-41.
 39. Huang SH, O’Sullivan BJCtoio. Overview of the 8th edition TNM classification for head and neck cancer. 2017;18:40.
 40. Wong KH, Panek R, Bhide SA, Nutting CM, Harrington KJ, Newbold KLJTBjor. The emerging potential of magnetic resonance imaging in personalizing radiotherapy for head and neck cancer: an oncologist's perspective. 2017;90:20160768.
 41. McJury M, O'Neill A, Lawson M, McGrath C, Grey A, Page W, et al. Assessing the image quality of pelvic MR images acquired with a flat couch for radiotherapy treatment planning. 2011;84:750-5.
 42. Zhang B, Tian J, Dong D, Gu D, Dong Y, Zhang L, et al. Radiomics features of multiparametric MRI as novel prognostic factors in advanced nasopharyngeal carcinoma. 2017;23:4259-69.





จุฬาลงกรณ์มหาวิทยาลัย
CHULALONGKORN UNIVERSITY

VITA

NAME Titiya Jirawatwanith

DATE OF BIRTH 28 March 1993

PLACE OF BIRTH Bangkok, Thailand

INSTITUTIONS ATTENDED 2012- 2015 The Degree of Bachelor of Science Program in Radiological Technology (First Class Honors), Faculty of Medical Technology, Mahidol University

HOME ADDRESS 18/450 Wish@Samyan Si Phraya Rd., Maha Phruttharam, Bang Rak, Bangkok 10500

PUBLICATION Jirawatwanith T, Tangyoosuk T, Lertbutsayanukul C, Jittapiromsak N and Rakvongthai Y. A Potential Biomarker from Diffusion Weighted Imaging and Parametric Response Map Analysis for Treatment Response Prediction in Nasopharyngeal Cancer. In proceeding of the 3rd Annual Scientific Meeting on Medical Physics and Biophysics (PIT-FMB) in conjunction with the 17th South-East Asia Congress of Medical Physics (SEACOMP), Journal of Physics 1505 (2020) 012032, August 8-10, 2019, Indonesia.